QUADRUPOLE ION ENTRANCE MASK STUDY

N. Ierokomc & M.R. Ruecker
The Perkin-Elmer Corporation
Aerospace Division
2855 Metropolitan Place
Pomona, California 91767

April 1971
Interim Report for April 1971
Revised Final Submittal

Prepared for
GODDARD SPACE FLIGHT CENTER
Greenbelt, Maryland 20771

STANDARD TITLE PAGE

1. Report No.	2. Government Accession No.	3. Recipient's Catalog No. 30001
4. Title and Subtitle QUADRUPOLE ION ENTRANCE MASK STUDY		5. Report Date April 1971
		6. Performing Organization Code
7. Author(s) N. Ierokomos & M.R. Ruecker		8. Performing Organization Report No.
9. Performing Organization Name and Address The Perkin-Elmer Corporation Aerospace Division 2855 Metropolitan Place Pomona, California 91767		10. Work Unit No. 11. Contract or Grant No. NAS5-11185
12. Sponsoring Agency Name and Address Goddard Space Flight Center Greenbelt, Maryland 20771		13. Type of Report and Period Covered STUDY REPORT April 1971 14. Sponsoring Agency Code

15. Supplementary Notes

16. Abstract

This report covers theoretical and computer analysis of the unstable ions in a quadrupole mass spectrometer. It covers the use of ion source masking to eliminate penetrating unstable ions. The test results of ion source nozzle masking with the associated decrease in peak tails are also included.

17. Key Words (Selected by Author(s))	18. Distribution Statement		
19. Security Classif. (of this report) UNCLASSIFIED	20. Security Classif. (of this page) UNCLASSIFIED	21. No. of Pages 70	22. Price*

TABLE OF CONTENTS

LIST OF ILLUSTRATIONS

LIST OF ILLUSTRATIONS (Cont)

SUMMARY

This report describes a technique of masking the exit aperture of an ion source which is used with a quadrupole mass filter to eliminate ions that would normally contribute to the tails appearing on either side of the mass peaks. It covers theoretical analysis, extensive computer analysis and experimental results.

These analyses and investigations show that the peak tails can be reduced by masking out ions with small initial transverse velocities or with small initial positions. The computer data that was obtained provided information on the relationships between all of the determining parameters that affect the amplitudes of unstable ions in the quadrupole field and the resulting intensities of the tails. These variables include the initial transverse velocity of the ions, its initial position, the initial phase of the radio frequency voltage, as well as the combination of radio frequency and direct current voltages, radio frequency, and ion energy. From the computer data an empirical relationship between the mass configuration and the tail intensity is developed.

Experimental results were obtained for the same instruments with and without masking. These results show a significant reduction in the tails by the utilization of the mask, which eliminates small initial positions. The results were also in close agreement with the analytical predictions.

INTRODUCTION

The qualitative understanding of quadrupole mass filter operation has been somewhat less than complete, particulary insofar as the tails on the peaks are concerned. In the past both theoretical and computer techniques were employed to gain a better understanding of quadrupole operation, but the primary concern has been the stable mode of operation. Such analyses provide information concerning ion transmission efficiency, peak shape (top-to-base ratio) and tradeoffs between sensitivity and resolving power.

Another important parameter in mass spectrometer operation is crosstalk, that is, the ion current contribution that one mass makes in the scan at the point where a second mass would normally be observed. This is a particularly important parameter in

applications where a wide dynamic range is required in a given mass scan. In these cases the peak tails are a determining factor. The following analysis, theoretical, numerical and experimental, is directed toward gaining a better understanding of peak tails and methods that can be utilized to reduce them.

THEORETICAL ANALYSIS

Quantative theoretical analysis of the quadrupole mass filter must be based upon the mathematics that describes the motion of ions in the quadrupole field. The ion trajectories are described by the Mathieu differential equations of motion, which are presented below for reference:

$$\frac{d^2x}{dz^2} + (a + 2q \cos 2z)\ x = 0 \qquad (1)$$

$$\frac{d^2y}{dz^2} - (a + 2q \cos 2z)\ y = 0 \qquad (2)$$

where

$$a = \frac{8eVdc}{mr_o^2\omega^2} \quad (3) \quad q = \frac{4eVac}{mr_o^2\omega^2} \quad (4) \quad z = \frac{\omega t}{2} \qquad (5)$$

The solutions to these differential equations are either stable or unstable, depending upon the exact values of the parameters a and q. This stability information is usually presented in the form of a stability diagram such as the one shown in Figure 1. The b_1 and a_0 curves shown in Figure 1 are the X and Y stability boundaries respectively. The region contained between these two boundaries is that of stable operation for both x and y motion. The region below the a_0 curve is unstable for the y motion while the region above the b_1 curve is unstable for x motion. Since there are two separate equations of motion that govern the path of the ion through the quadrupole field the stability diagram must actually indicate the stability of each of them. The lower quadrant of the stability diagram governs the stability for the y equation of motion while the upper quadrant governs the stability for the x equation of motion. Since only the signs of a and q differ between the x and y equations of motion simplifying the stability diagram is possible by superimposing the two stability criteria. This results in the typical stability

diagram that is shown in Figure 2. Four regions of stability are shown: region 1 represents an x unstable, y unstable condition, region 2 depicts an unstable region for both X and Y axes, region 3 is a y stable, x unstable region, while region 4 is a stable region in both X and Y axes.

The scan line that is shown in Figure 2 represents the path along which the parameters a and q must vary when a mass scan is accomplished by a variation of either frequency or rod voltage, where in the latter case the direct current (dc) to alternating current (ac) voltage ratio is presumably held constant. Observing the stability diagram, note that the width of a mass peak will be proportional to the width of the stable region at the point where it is cut by the scan line. Also, note that as the direct current to alternating current voltage ratio is increased the scan line will cut the stability diagram at successively narrower points, finally reaching the apex at which point the theoretical peak width is at zero and, hence, the theoretical resolving power infinite.

Unfortunately, however, this ideal condition can only be realized by an infinitely long quadrupole field. It is possible for unstable ions to traverse a quadrupole field of finite length, provided that the amplitudes of the unstable ions do not grow sufficiently fast to strike the field boundary before traversing the field length, as shown in Figure 3. The trajectories shown are for the y-z plane. Trajectories in the x-z plane also grow in amplitude, however, they cross the axis with each two cycles of the radio frequency field. For a given set of operating parameters for the quadrupole, that is, given values of z and q the rate of increase in amplitude of an ion as it progresses through the quadrupole field is controlled by the initial conditions of the ion at the point of entry into the field. These initial conditions are its initial transverse amplitude, its initial transverse velocity and the initial phase of the radio frequency field component at the time of entry. The exact values of a and q also determine the rate of increase in the amplitude of an ion. As the working point (a, q values) moves away from the stability boundary along the scan line the degree of instability of the ion increases and therefore, the amplitude grows faster. As a result, fewer and fewer ions will have the sufficiently favorable initial conditions required which will allow them to be transmitted through the field and, consequently, the amplitude of the ion current reaching a collector at the end of the field will diminish resulting in a tail on the mass peak. This effect is shown in Figure 4. Note that the tail on the y side of the peak is shown somewhat larger than the one on the x side of the peak. This is due to the skewed nature of the stability diagram and the differences in the detailed dependence of stability upon the parameters a and q for the two separate x and y motions.

Physically, the qualitative aspects of ion stability can be explained as follows: In the case of ion motion in the x and z plane the direct current potential components become increasingly positive as the ions approach the field boundary, that is, the quadrupole rods. As a result, the positively charged ions are stable and oscillate about the quadrupole axis. As the radio frequency component of the field increases, indicating an increasing value of q, the ions are acted upon by the alternating current component of the field. Since the field gradient increases with increasing x, an ion could possibly receive a net positive directed impulse over one cycle of the radio frequency. Therefore, as the amplitude of this net positive impulse increases, overcoming the negative force caused by the direct current field component is possible. As a result the ion motion can become unstable. The degree of instability will increase with higher and higher values of the radio frequency field component.

In the case of ion motion in the y-z plane, the direct current field potential decreases as the distance from the quadrupole axis becomes greater. In this case, when the alternating current component of the field is zero, that is when q is equal to zero, the ions are unstable. As the value of the alternating current field component increases, the ions could possibly receive a net negative impulse over one cycle of the field and in a similar way as for motion, therefore, the ion motion could become stable. In both the x and y motions the basic characteristic is a high frequency oscillatory action, resulting from the immediate action of the radio frequency field and a superimposed envelope, which is the result of successive positive or negative impulses given to the ions. In both cases, as the ions approach the field boundary (i.e., the quadrupole rods) they receive stronger impulses and are therefore turned around. However, as the ions approach the axis they receive successively weaker impulses and finally the action of the direct current field component will again begin to prevail. For unstable x and y ions the action of the alternating current and direct current field components, respectively, predominate causing the amplitudes to continue to grow. Therefore, considering a mechanical analog to the action of the quadrupole field is also helpful. This can be expressed in terms of a spring mass system where the spring constant is positive for stable oscillations and negative for unstable oscillations. The absolute value of the spring constant increases as the working point of the system moves away from the stability boundary.

There are several conventional techniques which are employed to reduce peak tails in a quadrupole mass filter. Observing Figure 3, note that the amplitude of unstable ions increase with each radio frequency cycle of the field. This fundamental fact is also clear from the form of the Mathieu differential equation in which the only time

dependence is a cos $\omega t/2$. Therefore, if the number of cycles that an ion spends in the quadrupole field can be increased, the probability of rejection of the ion will also be increased. The number of cycles that the ion spends in the outer field can be expressed in terms of the frequency of field oscillation and the time that the ion spends in the field:

$$n = \frac{\omega t}{2\pi} \tag{6}$$

The time that the ion spends in the field will be the function of the length of the field and the velocity component which the ion has in the direction of the field axis:

$$T = \frac{L}{v} \tag{7}$$

Combining Equations (6) and (7) the number of cycles of the radio frequency field component can be expressed in terms of the frequency of the field variation, the length of the field and axial velocity of the ion:

$$n = \frac{\omega L}{2\pi v} = \frac{fL}{v} \tag{8}$$

The above expression is almost trivial, but it does show the three parameters which are conventionally varied in order to reduce quadrupole peak tails. The frequency of the radio frequency field variation can be increased, the length of the quadrupole field can be increased and the axial velocity of the ions can be decreased. There are severe limitations on the variation of each of these quantities. In the case of frequency, an increase in frequency requires a corresponding increase in voltage or a reduction in the rod spacing parameter r_o as indicated by Equation (4). The former will lead to significant increases in the power required to supply the radio frequency field and the latter will decrease the sensitivity of the instrument. Increasing the length of the field requires a longer quadrupole and this is generally not acceptable for similar type instruments. Field lengths on the order of three to eight inches are typically used and variations much beyond these limits are clearly not compatible with the constraints of space flight instrumentation. A reduction in the actual velocity of the ions implies that the peak ion source must produce ions with a smaller energy spread. This is possible but only at the expense of ion source sensitivity. In summary, each of these parameters has been exercised to the limiting extent on previous quadrupole designs. The purpose of the current study was to investigate new methods for reducing quadrupole peak tails.

A detailed analysis, covering the motion of unstable ions in a quadrupole field and the resultant contribution to peak tails made by these ions, is presented in Appendix A. The reader is referred to this appendix to gain a detailed understanding of the quantative aspects of this problem. Only the high points of the analysis will be reviewed. The solution of Equations (1) and (2), in the unstable region of the stability diagram, take the form given below:

$$y = Y_1 e^{\mu z} f_1 (a,q,z) + Y_2 e^{-\mu z} f_2 (a,q,z) \qquad (9)$$

where Y_1 and Y_2 are constraints which are functions of initial conditions and f_1 and f_2 are complicated functions in z. The parameter is called the stability parameter and is a function of a and q. This parameter is equal to zero on the stability boundary and increases in value as the working point moves away from the stability boundary into a region of greater instability. The y equation of motion has been selected for discussion, but the same basic principles apply to the x motion as well. The constants Y_1 and Y_2 can be solved for in terms of the initial conditions. After the Y_1 and Y_2 constants are solved, using Equation (9) and its derivative, they can then be substituted into Equation (9). At the same time dropping the Y_2 term is possible because it is a dying exponential and does not appreciably affect the trajectory amplitude as the ions near the ends of the quadrupole field. Furthermore, since the transmission criteria for any ion trajectory will depend upon the maximum amplitude, which is achieved during transit, the fine details of the high frequency oscillations in the motion can be ignored. The following expression then provides the maximum value of the trajectory at some point in time:

$$y_{max} = \left[A(a,q,\phi)y(o) + B(a,q,\phi)y'(o)\right] C(a,q)e^{\mu\omega t/2} \qquad (10)$$

where y(o) is the initial transverse position,

y'(o) is the initial transverse velocity, and

ϕ is the initial phase angle of the RF field.

As indicated, the constants A and B are functions of a, q, and ϕ. The constant C is a function of a and q only and results from the maximum value achieved by the function f_1.

Studying Equation (10) it is clear that the qualitative effects which have been discussed in the preceding paragraphs are mathematically described. For example, the maximum amplitude that is achieved at some

point in time is a function of the initial conditions as predicted, the amplitude increases with ωt and the amplitude also increases with larger values of μ. The constants A, B and C, while also dependent upon the working point in the stability diagram, do not vary nearly as rapidly as the exponential term. Since interest is usually focused in a rather small region of the stability diagram, especially for high resolution work, the values of a and q are typically considered to have the same value as the apex of the stability diagram. To first order then, the constants A and B can be considered to be only functions of ϕ and the constant C can be just that, a constant.

For the computer work that was conducted later the initial position and initial transverse velocity were conveniently normalized, using the parameters η and γ as defined below:

$$\eta = \frac{y(o)}{r_o} \tag{11}$$

$$\gamma = \sqrt{\frac{V_I}{V_{ac}}} \sin \alpha \tag{12}$$

where r_o is the distance from the quadrupole axis to the field boundary, V_I is the initial ion energy, and α is the angle that the ion trajectory makes with the quadrupole axis at the point of entry. (For a quadrupole mass spectrometer employing quad bias, V_I is the ion energy at the point of injection into the quadrupole field.)

Using these definitions the following expression can be written for the maximum value of the ion trajectory at a point ωt:

$$Y_{max} = \left[A'(\phi)\eta + B'(\phi)\gamma\right] e^{\mu\omega t/2} \tag{13}$$

where the primes indicate that the constant C has been absorbed into the constants A and B. Note also that the constants are now shown to be only functions of ϕ. The above equation provides a significant amount of information regarding the effect of various parameters upon the ion trajectories. Note that the maximum amplitude of an ion is proportional to η and γ. Note in particular that if η and γ are both equal to zero the maximum amplitude is also zero. This corresponds to an ion that enters the quadrupole field coincident with axis and with no transverse velocity. Returning to Equations (1) and (2), note that these results would be expected.

Considering for a moment the effects of η and γ independently the above equation shows that if their values can be limited so that they are always above certain minimum levels then a guarantee that the maximum value of y will be greater than r_o may be possible before the ion reaches the end of the field. This depends of course upon the assumption that there are finite minimum values for A' and B'. In fact, as shown in Appendix A, this is true for the latter but not for the former. This presents no immediate difficulty for the present discussion. What is accomplished in effect, by restricting the values of η and γ as indicated, is to eliminate those ions which can contribute to tails before they enter the quadrupole field. For η, its value can be limited by placing a mask across the entrance aperture through which the ions enter the quadrupole field. By forming the mask in the shape of a cross those ions that would normally enter close to the x and y axes can be eliminated. Ions with larger values of η would normally be rejected anyway because they achieve greater maximum amplitudes as indicated by the above equation. An η mask is shown in Figure 5..

Limiting the minimum value of γ by using the mask technique requires some type of known functional dependence between γ and η. In this way the elimination of specific γ values by masking specified regions of the ions in the aperture could be guaranteed. While achieving a specified relationship between η and γ is possible, deflecting the ion beam prior to entering the aperture might also be feasible so that all ions would be guaranteed to have larger than a minimum value of γ. This of course leads to certain undesirable consequences with regard to the transmission of stable ions. Pursuing these individual factors at greater length is not necessary because by further examination of Equation (13) considering the effects of η and γ independently is clearly not possible. This is true because the entire quantity $A'\eta + B'\gamma$ controls the maximum amplitude of a given ion. For any given value of η and γ there may be a phase angle ϕ at which this quantity is zero and for which transmission can occur. Of more importance, however, is the range of ϕ over which transmission can occur for a given η and γ because $\Delta\phi/2\pi$ gives the transmission efficiency for that particular η and γ. This is expressed by Equation (14):

$$\Theta_{\eta,\gamma} = \frac{\Delta\phi(\eta,\gamma)}{2\pi} \qquad (14)$$

where Θ is the transmission efficiency for the given values of η and γ and $\Delta\phi$ is the range of phase angle over which transmission occurs.

The following expression can be found for $\Delta\phi$ by differentiating the quantity within brackets in Equation (13) and applying the restriction that y_{max} must be less than or equal to r_o in order for transmission to occur:

$$\Delta\phi = \frac{r_o \, e^{-\mu\omega t/2}}{\eta \frac{dA'(\phi)}{d\phi} + \gamma \frac{dB'(\phi)}{d\phi}} \qquad (15)$$

where the deriviatives of A' and B' are evaluated at the point where the expression within brackets in Equation (13) is equal to zero. Equation (15) is only valid under the assumption that $\Delta\phi$ is fairly small. This will be true except when the denominator of Equation (15) goes to zero since the numerator is very small. Actually Equation (15) must be multiplied by a factor of four in order to give the total transmission $\Delta\phi$ for a given η and γ, because both positive and negative values of ϕ (Equation 13) is double valued in ϕ when set equal to zero. Continuing with this analysis to the point of obtaining quantative results is not intended and, therefore, the factor of four can be ignored for the purposes of the present discussion.

The values of A' and B' can be determined for approximate expressions for A, B and C presented in Appendix A. Since these are complex functions of ϕ and sine, the entire function depends upon both η and γ, questioning the true value of ion entrance aperture masking is necessary. But observing Equation (15) note that, in general, for smaller values of η and γ, $\Delta\phi$ will be larger thereby implying a higher transmission of unstable ions by virtue of Equation (14). This conclusion can also be drawn by an inspection of Equation (13). As the values of η and γ increase, there is a narrower acceptable range of A' and B' which will cause the term in brackets to be small enough so that the maximum value y is less than r_o. For smaller values of η and γ, a wider range of A' and B' can be tolerated and still achieve ion transmission. This in turn implies a larger value for $\Delta\phi$.

The complete expression for the intensity of the tail on a quadrupole mass peak, under a particular set of operating conditions, is found by integrating Equation (14) over all values of η and γ. This is expressed in Equation (16):

$$\Theta_T = \frac{1}{2\pi\eta_o\gamma_o} \int_{\gamma_o} \int_{\eta_o} \Delta\phi(\eta,\gamma) \, d\eta \, d\gamma \qquad (16)$$

where η_o and γ_o denote the ranges of these particular parameters which are admitted into the quadrupole field. Considering Equations (15) and (16) together, the computational task becomes rather prodigious if a complete analytical solution is sought. As shown earlier, however, if the minimum values of η and γ can be limited, reducing $\Delta\phi$ is possible, which would reduce the size of the tails.

The question that must be answered now is, will an ion entrance aperture mask, of the type described earlier, be effective in limiting γ values? In a typical axially symmetric ion focusing system the statement that ions with positions closer to the axis will make smaller angles with the axis is generally true. In fact, this is a condition that is satisfied by the well known paraxial ray equation. In ion focusing systems that have aberrations and, in particular, spherical aberrations, it is possible for the ion trajectories to cross in such a way that ions lying nearer the axis will have larger angles. Even so, it appears that an η mask may be effective in eliminating a reasonable percentage of the ions with smaller γ values. It was decided that this probability was high enough to continue the investigation experimentally and by computer.

Before discussing the computer investigations and the subsequent experimental results, consideration of the magnitudes involved in the quantities that have been dealt with in the foregoing equations will be useful. In particular, the value of $\mu\omega t/2$ is of great importance since it appears as an exponential factor and, therefore, has a large affect upon the magnitude of the maximum value of an ion trajectory. Using Equations (4) and (7) along with the relationship between the velocity of axial lines and their corresponding kinetic potentials, the following expression is obtained:

$$\frac{\mu\omega t}{2} = \mu \frac{L}{r_o} \sqrt{\frac{1}{2q} \frac{V_{ac}}{V_o}} \qquad (17)$$

where q is the apex value of the stability parameter and V_o is the axial component of the kinetic energy potential of the ions as they travel in the quadrupole field. The value of μ has been related to the distance from the stability boundary and units of theoretical peak base width (see Appendix A) and this expression is given in Equation (18):

$$\mu \simeq 0.97 \sqrt{t \frac{\Delta m}{m}} \qquad (18)$$

where the parameter t is the number of theoretical peak base widths away from the stability boundary for a theoretical resolution of $\Delta m/m$, the theoretical peak base width is the base width without tails and the theoretical resolution is the resolution without tails. Combining Equations (17) and (18) provides an easy to use expression for $\mu\omega t/2$ and is given in Equation 19:

$$\frac{\mu\omega t}{2} = 0.82 \frac{L}{r_o} \sqrt{t \frac{\Delta m}{m} \frac{V_{ac}}{V_o}} \qquad (19)$$

where the appropriate numerical value for q has been substituted.

Note that Equation (19) is dimensionless, as it should be, with dimensioned parameters appearing as ratios. A typical set of parameter values is given below for the instrument under investigation along with the resulting value for $\mu\omega t/2$:

$$\frac{L}{r_o} = 25 \qquad \text{(effective value)}$$

$$V_{ac} = 400 \text{ V}$$

$$V_o = 20 \text{ V}$$

$$\frac{\Delta m}{m} = \frac{1}{40} \qquad t = 1$$

therefore,

$$\frac{\mu\omega t}{2} = 14.5 \rightarrow e^{-\mu\omega t/2} \simeq 5 \times 10^{-7}$$

The resulting value of the exponential term is extremely small and indicates that significant tails should not be observed, according to the above theory, even without an entrance aperture mask. Some approximate calculations were attempted and these gave smaller values for Θ_T than observed in the experimental results. The reasons for this are not entirely understood but one possible contributing factor that may explain this disparity, results from the details of the interaction of the quadrupole field with the ions as they enter the field. Brubaker, for example, showed the importance of the field geometry in the entrance region in enhancing the transmission of stable ions. The transmission of unstable ions may also be similarly improved, over theoretical expectations, due to the entry process.

In conclusion, while attempts to perform a complete theoretical analysis of the magnitude of tails on the quadrupole mass peaks, in terms of the transmission properties of the quadrupole field in the unstable region, were not entirely successful, they did provide insight into the possible advantages of the use of ion entrance aperture masking and laid the ground work for the computer investigations and the experimental results that are presented in the following two sections.

COMPUTER ANALYSIS

Computations of the ion trajectories were run for ions which theoretically are unstable in their y axes. The variable parameters considered were 100 and 200 resolution; 5, 20, and 100 percent of peak width from the stability region; various η and γ values and various phase values. The computer program is normalized to the particular quadrupole so that when the amplitude of the ion oscillations reach unity the ions would impact into the rods, thus being stopped. The limit of motion in the z direction (parallel to the length of the rods) was taken at 16,000 degrees or 44.4 cycles.

Tabulation of points of ion impact, in degrees, or highest amplitude at 16,000 degrees are given in Table 1 for some of the computer runs. Using this table note that γ has a greater effect than η upon the trajectory of an ion. This difference for low values of η and γ however, is only on the order of twenty-five percent.

In order to more readily visualize the behavior of the ions for the given parameters, several charts were made and are presented in the accompanying figures. The plots show only the upper boundary of the trajectory envelopes. Figure 6 shows the trajectories for several initial phases with given values of η and γ for 5, 20, and 100 percent of Δq (where Δq = peak width at a given resolution). The above figure is a plot of resolution 200, but using Table 1 note that the points of impact for resolution 100, at the same values of η and γ, are not drastically different from the values for resolution 200. The difference appears to be on the order of the square root of resolution, as stated in the previous section.

Figure 6 is the actual maximum trajectory envelope. From this figure note that the maximum amplitude for $\gamma = 0$, $\eta > 0$ unstable ions is at approximately 90 degrees and approximately 270 degrees phase angle. For ions with initial $\gamma > 0$, $\eta = 0$ the maximum amplitude is at about 180 degrees with minimum at zero degrees.

TABLE 1. POINTS OF ION IMPACT

INITIAL PHASE (°)	η	γ	PERCENT FROM STABILITY (°)	RESOLUTION	Z-AXIS POSITION (°)	AMPLITUDE
0	0	0.0314	5	100	4,141	1.0782
0	0	0.0314	5	200	4,141	1.0707
90	0	0.0314	5	100	3,062	1.0884
90	0	0.0314	5	200	3,062	1.0854
180	0	0.0314	5	100	2,342	1.0881
180	0	0.0314	5	200	2,342	1.0878
270	0	0.0314	5	100	3,062	1.0478
270	0	0.0314	5	200	3,062	1.0453
0	0	0.0314	20	100	3,782	1.0513
0	0	0.0314	20	200	3,782	1.0202
90	0	0.0314	20	100	3,062	1.1357
90	0	0.1314	20	200	3,062	1.1162
180	0	0.0314	20	100	2,343	1.1130
180	0	0.0314	20	200	2,343	1.1039
270	0	0.0314	20	100	3,062	1.1900
270	0	0.0314	20	200	3,062	1.0728
0	0	0.0314	100	100	3,063	1.0419
0	0	0.0314	100	200	3,063	1.0389
90	0	0.0314	100	100	2,703	1.1613
90	0	0.0314	100	200	2,703	1.1601
180	0	0.0314	100	100	2,343	1.2498
180	0	0.0314	100	200	2,343	1.2504
270	0	0.0314	100	100	2,703	1.0947
270	0	0.0314	100	200	2,703	1.0938
0	0.0025	0	5	100	--	--
0	0.0025	0	5	200	15,660	0.0116
0	0.0025	0	20	100	15,661	0.0599
0	0.0025	0	20	200	15,661	0.0358

TABLE 1 (Concluded)

INITIAL PHASE (°)	η	γ	PERCENT FROM STABILITY (°)	RESOLUTION	Z-AXIS POSITION (°)	AMPLITUDE
0	0.0025	0	100	100	13,502	1.0464
0	0.0025	0	100	200	13,502	1.0320
90	0.0025	0	5	100	--	--
90	0.0025	0	5	200	15,661	-0.5028
90	0.0025	0	20	100	14,581	-1.0404
90	0.0025	0	20	200	15,661	-0.9322
90	0.0025	0	100	100	8,822	-1.1694
90	0.0025	0	100	200	8,822	-1.1678
180	0.0025	0	5	100	--	--
180	0.0025	0	5	200	15,660	0.0058
180	0.0025	0	20	100	15,661	0.0292
180	0.0025	0	20	200	15,661	0.0175
180	0.0025	0	100	100	15,302	1.1022
180	0.0025	0	100	200	15,302	1.0820
270	0.0025	0	5	100	--	--
270	0.0025	0	5	200	15,661	0.5129
270	0.0025	0	20	100	14,221	1.0047
270	0.0025	0	20	200	15,661	0.9628
270	0.0025	0	100	100	8,462	1.0847
270	0.0025	0	100	200	8,462	1.0829

$$\eta = \frac{y(o)}{r_o}$$

$$\gamma = \left(\frac{V_I}{V_{ac}}\right)^{1/2} \sin \alpha$$

where:

$y(o)$ = initial position of ion

r_o = half the distance between rods

V_I = injection energy of ion

V_{ac} = RF potential at rods

α = entrance half angle

Before involvement of phase, it would be of interest to determine the intensity of tails with some actual expected parameters. Figure 7 shows the geometry of the actual quadrupole.

In order to determine the amplitude of any ion, the number of cycles N (or $\omega/2\pi$) the ion spends within the quadrupole must first be calculated.

To do this, the following must be known:

a. Mass of ion M

b. Velocity of ion

c. Length of quadrupole L

d. Separation of rods r_o

e. Frequency ω_f

The velocity of the ion is given by

$$V = 1.39 \times 10^6 \sqrt{\frac{E_v}{M}} \quad \text{cm/sec.} \tag{20}$$

where E_v is the energy of the ion in electron volts (ev). Let:

$E_v = 10$ ev

$L = 15.24$ cm

$r_o = 1$

$M = 50$

$\omega_f = 1.5$ MHz

giving

$$V = 1.39 \times 10^6 \sqrt{\frac{10}{50}} \simeq 0.63 \times 10^6 \text{ cm/sec}$$

since

$$t = \frac{L}{V} = \frac{15.24}{0.63 \times 10^6} \simeq 24 \times 10^{-6} \text{ sec} \tag{21}$$

therefore the number of cycles an ion spends in the quadrupole is

$$N = t\omega_f \qquad (22)$$

$$= (24)\ (1.5) = 36 = 12{,}960°$$

Armed with the number of cycles for a typical ion, analyzing amplitudes and intensities for given η, γ and ϕ is now possible using the computer runs.

The design of the existing quadrupole is such that the maximum γ is about 0.02 (for an angle of $\alpha = 1°10'$). The maximum η is about 0.025, equivalent to a 0.01 inch diameter nozzle. The ion distribution as a function of η or γ is assumed to be as shown in Figures 8A and 8B. Figure 9 shows the trajectories (maximum amplitude) for different values of η and ϕ at zero γ.

Having assumed a constant distribution of γ and η of the ions entering the quadrupole, using the data presented in Figures 6 and 9 and other computer runs it is possible to establish the amplitude variations of a given ion with respect to phase. This phase, is the phase that the radio frequency is at when the ion enters the quadrupole.

Once the phase-amplitude relationship is established, then obtaining the transmission of the unstable ions or peak tail intensity is not very difficult. From Figure 9 note that at the end of the quadrupole Z-axis (12,960°), only ions with an η value of 0.005 or smaller are transmitted 100 percent and at all phases. This is concluded because the 90 and 270 degree phase ions, which have the maximum amplitude, are just hitting the rods at the end of the quadrupole. The value of maximum η at 100 percent transmission (0.005 in this case) is herein referred to as the maximum detectable η.

From the computer acquired data, deriving Figure 10 was possible, which is simply the amplitude of a given ion with variations of entrance phase and every other parameter being constant. The shape of the amplitude phase relationship is approximately a slightly offset sinusoidal wave crossing the zero level at between three to eight degrees and 170 to 178 degrees. This crossing of the zero level is very important, because ions with finite initial amplitude will be forced to decrease their amplitude and eventually allow this amplitude to go to zero. Figure 10 shows that this zero crossing holds for all values of η.

Figure 10 is also divided into three regions. Region I which is always smaller than $\pm r_o$, indicates the transmission of all ions with η value up to and including maximum detectable (η_{MD}) irrespective of initial phase. Region II will transmit ions of η maximum with initial phase within the bandwidth shown as ϕ_T. Ions with η values less than the maximum will have an increasing bandwidth as η approaches η_{MD} at which time the passable bandwidth is 100 percent. Region III is a region where ions are impacting the rods.

Having a constant intensity distribution with respect to η (Figure 8A) and with respect to phase, determination of the percent transmission (tail amplitude) of unstable ions with γ equal to zero is now possible.

Figure 11 shows the percent contribution of each of the above regions. This figure shows that for a resolution of about 200, a Δq of twenty percent, an ion mass of 50, an ion energy of ten electron volts and an alternating current frequency of 1.5 MHz, there is a thirty-four percent transmission of unstable ions. From this figure, predicting the decrease in tail amplitude is also possible if a nozzle mask was used to eliminate all ions up to a certain value of η. Two mask sizes are considered in this figure, with the appropriate total tail intensity shown below the intensity plot. Figure 12 is similar to Figure 10 except that it shows the amplitudes for ions at $\Delta q = 5\%$. Since the ions are more stable at that point, a larger value of η is therefore detectable. After rearrangement of the data Figure 13 is obtained showing the total tail intensity. Similar treatment of the ions at $\Delta q = 100\%$ is presented in Figure 14. The change in tail intensity as a function of Δq (for $\gamma = 0$) is shown in Figure 15. The conclusion reached from the above data is that the size of the mask under the conditions stated above need not exceed an η value of 0.0075 or 0.003 inch. A higher η mask will of course decrease the tails further, but will also decrease the total intensity by blocking more of the nozzle aperture. All of the above tail data is with ions having $\eta > 0$ values but no γ value, or no side energy.

In order to correctly analyze the tail data, all ions must be allowed to assume any value of γ from zero to some maximum. As a first step again, the ion amplitudes will now be considered with η value equal to zero. This is done in order to simplify the problem before combining the two effects.

Figure 16 shows the amplitudes as a function of γ in a similar form as Figure 9 for η. This figure is for $\Delta q = 20\%$ and resolution of 100. The amplitude for a resolving power of 200 is not too different from that at 100.

Data was run at different phases to obtain the change of amplitude as a function of phase, which is given in Figure 17. The total tail intensity at $\Delta q = 20\%$ is shown in Figure 18. The tails are considerably smaller in the γ parameter than in the η , 14.5% for $\gamma > 0$; $\eta = 0$, 34% for $\gamma = 0$; $\eta > 0$ and at a $\Delta q = 20\%$. If a γ mask was used (masking of the ion source) it appears that the tails could be reduced considerably without much reduction of the total ion intensity. Final comparison of tail reduction, however, must be made with a combination of γ and η.

The combination of amplitude contributions of η and γ with respect to phase appears to be a linear combination. To provide a clearer visualization of this fact, the data has been plotted on a polar coordinate plot (Figure 19). This plot shows the η and γ components and the resultant from combining these components.

This figure is for positive η and γ values. The η contribution of the ion amplitude is negative between the phase angle of approximately twelve to 170 degrees. This negative amplitude portion will offset the always positive γ contribution between the above phase angles. Thus, the resultant amplitude for a phase angle of about ninety degrees and equal η and γ contribution will be zero at the end of a quadrupole. This will result in those ions transmitted as tails. At phase angles greater than 180 degrees the two component contributions are both positive and as such will result in large amplitude of motion for the ions. In Figure 19 the amplitude is the result of only 3,782 degrees down the Z-axis or somewhat over one-fourth the length of the quadrupole. As the Z-axis length is allowed to increase, the amplitudes shown in Figure 19 will also grow exponentially but will maintain the phase distribution as shown.

Equal values of η and γ were chosen to show the relative contribution of the two parameters. The resultant can be approximated when γ is equal to or greater than η, by

$$A_y = a(1-k' \cos(k\phi)) \qquad (23)$$

$$\text{if } \gamma \geq \eta$$

where a,k' and k are functions of γ and η. When $\gamma = \eta$ then $k \simeq 0.75$ and takes the value of unity when $\gamma >> \eta$. The general equation for ion amplitude is of the form

$$a = C\{N\gamma\,(1 + |\sin\tfrac{\phi}{2}|) + k\eta\,(1 - N\sin(\phi))\}e^{f(\omega,\mu,t)*} \qquad (24)$$

*This equation is derived from curve-fitting of the computer data but can be compared to the theoretical relationships of the previous sections.

where C is a function of resolution, Δq, r_o and N is the number of cycles an ion has spent in the quadrupole fields.

Figure 20 shows the ion amplitudes of the 0.003 inch mask (minimum η ions) and ion amplitudes of maximum η. It also shows the maximum detectable γ. The amplitudes at the maximum γ are too large to be shown here. In order to derive the total intensity of the tails, the ion distributions in ϕ, γ and η are taken independent of each other. This means that a given bandwidth ($\Delta\phi$, $\Delta\gamma$, $\Delta\eta$) contains the same number of ions as any other bandwidth of the same variable.

thus:

$$I_\phi = \frac{\Delta\phi}{2\pi};\ I_\gamma = \frac{\Delta\gamma}{\gamma_{max}};\ I_\eta = \frac{\Delta\gamma}{\eta_{max} - \eta_{mask}} \tag{25}$$

if I_o is the number of ions entering the quadrupole then

$$I_{tail} = I_o I_\phi I_\gamma I_\eta = I_o \left(\frac{\Delta\phi}{2\pi}\right)\left(\frac{\Delta\gamma}{\gamma_{max}}\right)\left(\frac{\Delta\eta}{\eta_{max} - \eta_{mask}}\right) \sim$$

$$I_o \int_0^{2\pi} \int_0^{\gamma} \int_{\eta_{mask}}^{\eta} d\phi\ d\gamma\ d\eta \tag{26}$$

a computer program was run with

$$\Delta\phi = \Delta\phi_{A \leq |1|};\ \Delta\gamma = 0.002;\ \Delta\eta = 0.002$$

where $A \leq |1|$ = ion amplitudes up to r_o

thus:

$$I_{s\ tail} = I_o \left(\frac{\Delta\phi}{360}\right)\left(\frac{0.002}{0.02}\right)\left(\frac{0.002}{0.025 - 0.0075}\right) =$$

$$0.0108\ I_o \sum_s \frac{\Delta\phi_s}{360}$$

The increment $\Delta\phi$, is the phase bandwidth within which the ions will pass through the quadrupole without hitting the rods (see Figure 21). Ions passing through with all possible phases will, obviously, possess a $\Delta\phi$ which is equal to 360. This means 100 percent transmission of those ions with respect to phase. Depending on initial conditions, ion trajectories, with respect to phase distribution will cross the rod displacement under one of these conditions:

a. Will not cross r_o = 100% transmission

b. Will cross r_o once = initial large γ small η, or small γ small η

c. Will cross r_o two times = initial large γ medium η.

d. Will cross r_o three times = initial small γ large η.

e. Will cross r_o four times = initial medium γ large η or small γ medium η.

The computer run was such that the points of crossover, either positive or negative, were calculated for each ion under the given initial conditions. Knowing the phase at the crossover points and the general phase-amplitude distribution for η and γ, determination of phase transmission is relatively simple. By merely summing all the phase transmissions of all the $\Delta\eta$ and $\Delta\gamma$ increments the final amplitude of the tails can be obtained with any of the mentioned initial conditions. A test case was run for m/e 50 at a frequency of 1.5 MHz, a Δq = 20%, six inch quadrupole rods, ion energy of ten electron volts and a resolution of 200.

The equation used in this program is the amplitude equation given above with the initial conditions evaluated and the evaluation of amplitude equal to the absolute value of unity.

$$|1| = k_1 k_2 \gamma(1 + \sin\tfrac{\phi}{2}) + k_1\eta\ (1-k_3 \sin\phi) \tag{27}$$

giving

$$|1| = 216.5\gamma + 6.1\eta + 216.5\ (\gamma \sin\tfrac{\phi}{2} = \eta \sin\phi) \tag{28}$$

or

$$0.168 \geq |\eta + 36.1\ (\gamma + \gamma\sin\tfrac{\phi}{2} - \eta\sin\phi)| \tag{29}$$

The computer evaluated the above equation for all possible η and γ from known increments and solved for the phase ϕ. A sample of the data output is given in Figure 22.

The smallest phase increment with which the computer was calculating was a one degree increment. Such a large increment would cause the computer to miss a large number of crossover points which at the one degree increment were farther away from unity than the $|1.000 \pm 0.050|$ amplitude tolerance. By knowing the general shape of phase distribution of the trajectories, estimating the crossovers of almost all of the roughly 100 incremental combinations of η and γ was possible. From this data it was estimated that for the above mass (m/e 50) and under the above conditions, the Y-axis tail should be about twelve percent at twenty percent of Δq. When this is compared with empirical data, there is relatively good agreement.

TEST RESULTS

Prior to the computer data becoming available, the theory of masking the ion exit slit was tested in the laboratory. The mask utilized for the first attempt was a 0.001 inch cross of wires in front of the aperture. The test data did not appear to have a reduction of the tails. At this time the computer results for η amplitudes was obtained and the phase-amplitude relationship had been derived (as shown in Figure 10) which indicated that even with masking small η values, in this case a value of η equal to 0.0025, because of the zero amplitude at some phases there would always be tails. The data indicated that the tail reduction would be of approximate amplitude, as the total intensity decreased, because of masking.

After the derivation of the γ contribution of the phase-amplitude distribution (Figure 17) from the computer data note that the combination of η and γ could cause the tails to be reduced with a larger mask.

At this point the ion source investigation was temporarily halted and a five mil wire was installed on the nozzle. A single wire was installed and was aligned with the X-axis (positive rods) of the quadrupole.

Upon retest of the analyzer with the five mil wire mask installed and using a logarithmic electrometer the y peak tail reduction was actually apparent to the extent that the m/e 27 and 28 (y) valley was down significantly more than the m/e 28 and 29 (x) valley. Figures 23 and 24 are peak tail comparison scans with and without the mask. Resolution was still limited by the deterioration of the peak top at the higher resolving power. The quadrupole Vdc's were then reversed to observe the effect of the mask upon the x-tail. A dramatic x-tail reduction was noted here while increasing the y-tail back to the no-mask level as shown in Figures 25 and 26.

Testing with the five mil wire was limited because of the one axis affect and therefore, more productive testing was thought possible by changing to a 0.003 inch cross mask. This would then reduce both the x and y tails and also help to determine a threshold mask size. The five mil mask was replaced with this new configuration and data taken for comparison with the previous configuration (see Figure 27). Both x and y tails were reduced, however, the y-tail was not fully reduced. It was found that by reversing the rod direct current potentials that the y-tail was reduced adequately (see Figure 28). This meant that the mask alignment was not within a minimum tolerance requirement. Unfortunately, the direct current orientation where the y-tail was reduced the most had typically been a condition where the peak top was poor. In the past all quadrupoles have had a preferred rod direct current polarity orientation and this instrument was no exception, with the x-side peak top exhibiting similar degradation. This problem clearly had to be rectified if a good top-to-base ratio was to be obtained at the higher resolving powers.

Tests run with a masked source, flight-type quadrupole show extremely good results. A typical mass scan is shown in Figure 29. Note from this figure that the dynamic range is over six decades and the data is the best ever obtained under the same conditions for this type of quadrupole. The data is so improved as to allow the separation of the peaks of carbon dioxide and propane (see Figure 30). The minimum resolution required for such a separation is one part in 650. Resolving powers of over 750 could be obtained with this unit while sacrificing sensitivity. To improve the sensitivity the nozzle was redesigned to allow a higher intensity of ions to enter the analyzer region.

CONCLUSIONS

In the previous sections it was shown theoretically that by masking off small amplitude ions, a large reduction of peak tails would occur. Such a reduction improves the quadrupole operation in terms of better shaped peaks and increased resolution. These predictions were verified by experiment as the actual data in the test results section shows. Although considerable improvement was realized by the use of amplitude masking, including resolutions of close to 1,000, it is felt that by use of perhaps angle masking or some optimum combination further improvement can be made.

APPENDIX A

THEORETICAL ANALYSIS OF QUADRUPOLE PEAK TAILS

By M.R. Ruecker

Trajectory Analysis

The theoretical study of the tails on the peaks of a quadrupole mass filter must begin with an analysis of the equations of motion of ions in the quadrupole mass filter when the controlling parameters are such that the ion trajectories are unstable (i.e., unbounded). The equations of motion will be solutions to Mathieu's differential equation. Solutions to the Mathieu D.E. have been found for various regions of the stability diagram. Referring to Figure 1, the regions of interest for this analysis are first, below the a_o stability boundary (for y motion), and second, between the b_1 and a_1 stability boundaries (for x motion). The general expressions for the x and y equations of motion are[1]:

$$x = X_1 e^{\mu z} \sum_{r=-\infty}^{+\infty} c_{2r+1} e^{(2r+1)zi} + X_2 e^{-\mu z} \sum_{r=-\infty}^{+\infty} c_{2r+1} e^{-(2r+1)zi} \tag{30}$$

and

$$y = Y_1 e^{\mu z} \sum_{r=-\infty}^{+\infty} c_{2r} e^{2rzi} + Y_2 e^{-\mu z} \sum_{r=-\infty}^{+\infty} c_{2r} e^{-2rzi} \tag{31}$$

where X_1, X_2, Y_1, and Y_2 are constants determined by initial conditions.

---

[1] Theory and Application of Mathieu Functions, by N.W. McLachlan; Dover Publications, Inc., New York, 1964. Pages 84-85.

APPENDIX A

In order to have solutions that are real it is necessary to require that the c_{2r} are complex conjugates while the c_{2r+1} and c_{-2r+1} are also complex conjugates. Then Equations (30) and (31) can be rewritten:

$$x = X_1 e^{\mu z} \sum_{r=-\infty}^{+\infty} \left[f_{2r+1} \cos(2r+1)z - g_{2r+1} \sin(2r+1)z \right]$$

$$+ X_2 e^{-\mu z} \sum_{r=-\infty}^{+\infty} \left[f_{2r+1} \cos(2r+1)z + g_{2r+1} \sin(2r+1)z \right] \quad (32)$$

where $c_{2r+1} = f_{2r+1} + ig_{2r+1}$ and $c_{-2r+1} = f_{2r+1} - ig_{2r+1}$

with f_{2r+1} and g_{2r+1} real, and

$$y = Y_1 e^{\mu z} \sum_{r=-\infty}^{+\infty} \left[f_{2r} \cos 2rz - g_{2r} \sin 2rz \right]$$

$$+ Y_2 e^{-\mu z} \sum_{r=-\infty}^{+\infty} \left[f_{2r} \cos 2rz + g_{2r} \sin 2rz \right] \quad (33)$$

where $c_{2r} = f_{2r} + ig_{2r}$ and $c_{-2r} = f_{2r} - ig_{2r}$

with f_{2r} and g_{2r} real.

In the preceding equations μ is the stability parameter which approaches zero as the working point in the stability diagram approaches a stability boundary. The c_{2r} and c_{2r+1} are coefficients which are functions of 'a' and 'q', or as more often expressed, 'a', 'q', and μ.

At this point attention will be restricted to 'y' motion in the interest of space. This will not significantly reduce the resulting insight or information particularly since the tail on the y side of a normal quadrupole mass filter transmission peak is much larger than on the x side of the peak.

APPENDIX A

The next step in the analysis is to solve for the constants Y_1 and Y_2 in terms of the initial conditions. Equation (33) does not include the phase angle of the RF voltage which is one of the initial conditions. To include the effects of phase the following substitution is made in the sin and cos terms:

$$z = \frac{1}{2}(\omega t + \phi) \tag{34}$$

Then it is possible to solve for Y_1 and Y_2 in terms of the initial conditions y(o), y'(o) and ϕ in the conventional manner. The results are given below using simplified notation. Only the term will die out due to the decaying exponential factor. The result is:

$$Y_1 = \frac{A_{22}\, y(o) - A_{12}\, y'(o)}{D} \tag{35}$$

where:

$$A_{22} = -\omega \left[\mu \sum (fc + gs) + \sum r\,(fs - gc) \right]$$

$$A_{12} = \sum (fc + gs)$$

$$D = -2\omega \left[\left\{ \sum fc \right\}^2 - \mu \left\{ \sum gs \right\}^2 - \left\{ \sum fc \right\} \left\{ \sum rgc \right\} - \left\{ \sum gs \right\} \left\{ \sum rfs \right\} \right]$$

with:

$f = f_{2r}$, $g = g_{2r}$, $s = \sin r\phi$, $c = \cos r\phi$, r = integer

$$\sum = \sum_{r=-\infty}^{+\infty}$$

APPENDIX A

It is clear without going much further that the results are becoming very complicated. It is possible to make some observations regarding the factors which affect the ion trajectories in the unstable region of operation. Simplifying Equation (35), combining with Equation (33), and dropping the Y_2 term as previously indicated yields:

$$y \approx \left[A\, y(o) + B\, y'(o)\right] e^{\mu\omega t/2} \sum \left[f_{2r} \cos r(\omega t + \phi) - g_{2r} \sin r(\omega t + \phi)\right] \tag{36}$$

where A and B are functions of ϕ, a, q, μ, and ω.

The expression under the summation is bounded and therefore if a maximum value for y is considered the final simplified result is:

$$y_{max} \approx \left[A(\phi)\, y(o) + B(\phi)\, y'(o)\right] C\, e^{\mu\omega t/2} \tag{37}$$

where C is a constant which will depend only upon a, q, and μ. Note it is much easier to see the form of the effects controlling the trajectories in the unstable region. The envelope of the trajectory increases exponentially with distance down the quadrupole axis for distances which are far from the origin. The amplitude of motion at any point along the axis is proportional to a linear combination of multiples of the initial transverse position and velocity, and the multipliers are dependent upon the initial phase angle of the RF voltage.

Continuing the analysis it is necessary to gain sufficient insight into the parameters $A(\phi)$ and $B(\phi)$ such that simplifying assumptions can be made. Three special cases are of interest: Case 1 - $y'(o)$, Case 2 - $y(o) = o$, and Case 3 - $A(\phi)\, y(o) + B(\phi)\, y'(o) \approx 0$.

Before studying these special cases it will be useful to investigate the parameters $A(\phi)$ and $B(\phi)$. These are dependent upon the c_{2r} coefficients which appear in Equation (33). In keeping with the y motion analysis, the c_{2r} coefficients can be evaluated from the following recursion formula[2]:

$$\left[a - (2r - i\mu)^2\right] c_{2r} - q(c_{2r+2} + c_{2r-2}) = 0 \tag{38}$$

---

[2] Ibid. Page 83

APPENDIX A

Solving Equation (38) for c_{2r} yields:

$$c_{2r} = \frac{(c_{2r+2} + c_{2r-2})\, q \left[(a - 4r^2 + \mu^2) - i\, 4r\mu\right]}{(a - 4r^2 + \mu^2)^2 + 16r^2\mu^2} \qquad (39)$$

Making the substitutions:

$$A_{2r} = \frac{q(a - 4r^2 + \mu^2)}{(a - 4r^2 + \mu^2)^2 + 16r^2\mu^2} \qquad (40)$$

$$B_{2r} = \frac{4qr\mu}{(a - 4r^2 + \mu^2)^2 + 16r^2\mu^2} \qquad (41)$$

then

$$c_{2r} = (c_{2r+2} + c_{2r-2})(A_{2r} - i\, B_{2r}) \qquad (42)$$

Comparing the relative values of A_{2r} and B_{2r} it is seen that $A_{2r} >> B_{2r}$ since $B_{2r} \propto \mu$. The primary interest in the peak tails will be in the region within one mass unit of the stability boundary. Therefore, for high resolving power, again typically of interest, $\mu \leq 0.1$. This will be verified later. Then

$$A_{2r} \approx -\frac{q}{4r^2} \quad \text{for } r \geq 1 \qquad (43)$$

$$A_o \approx \frac{q}{a} \qquad (44)$$

$$B_{2r} = \frac{q\mu}{4\, r^3} \quad \text{for } r \geq 1 \qquad (45)$$

$$B_o = 0 \qquad (46)$$

This gives a clear indication of the relative values of A_{2r} and B_{2r}. This information can then be applied to establishing the relative values of the C_{2r} as well as the real and imaginary parts thereof.

APPENDIX A

There is no attempt here to make this analysis entirely rigorous from a mathematical point of view. Therefore, it is possible to make use of standard evaluation techniques to determine the relative values of the c_{2r}. Since the series expressions in Equation (33) are assumed to converge, it follows that each higher order value of f_{2r} and g_{2r} must be smaller than the preceding order.

The normal approach that is taken when computing the c_{2r} is to set one of the higher order c_{2r} equal to zero. For the purposes of our analysis we will chose $c_8 = 0$. Then from Equation (42)

$$r = 3 \quad c_6 \approx c_4 \, (A_6 - i \, B_6) \tag{47}$$

$$r = 2 \quad c_4 \approx c_2 \, (A_4 - i \, B_4) \tag{48}$$

$$r = 1 \quad c_2 \approx c_o \, (A_2 - i \, B_2) \tag{49}$$

where second order terms in A_{2r} and B_{2r} that appear in c_4 and c_2 have been omitted. Substituting Equation (49) into Equation (48) and the result into Equation (47) yields:

$$c_o = 1$$

$$c_2 \approx (A_2 - i \, B_2)$$

$$c_4 \approx (A_4A_2 - B_2B_4) - i \, (A_2B_4 + A_4B_2)$$

$$c_6 \approx (A_6A_4A_2 - A_6B_4B_2 - B_6B_4A_2 - B_6A_4B_2)$$
$$- (A_6B_4A_2 + A_6A_4B_2 + B_6A_4A_2 - B_6B_4B_2)$$

Using the approximate expressions for A_{2r} and B_{2r} given in Equations (43) through (45):

$$c_o = 1$$

$$c_2 \approx A_2(1 + \mu i)$$

$$c_4 \approx A_4A_2 \left[(1 - \tfrac{1}{2} \mu^2) + \tfrac{3}{2} \mu i\right] \approx A_4A_2 \left[1 + \tfrac{3}{2} \mu i\right]$$

$$c_6 \approx A_6A_4A_2 \left[(1 - 2 \mu^2) + \tfrac{5}{3} \mu i\right] \approx A_6A_4A_2 \left[1 + \tfrac{5}{3} \mu i\right]$$

and finally

$$c_o = 1$$

$$c_2 \approx -\frac{q}{4}(1 + \mu i)$$

$$c_4 \approx \frac{q^2}{64}(1 + \frac{3}{2}\mu i) \qquad (50)$$

$$c_6 \approx -\frac{q^3}{2304}(1 + \frac{5}{3}\mu i)$$

It is pointless to compute larger terms because they become extremely small. At this point it is significant to notice that the imaginary terms corresponding to the q_{2r} are smaller than the real terms by a factor of μ. (It is important to realize that the above approximations are only valid for small μ. As $\mu \to 1$ the expressions will become quite different.)

Having computed approximate values for the c_{2r}, and consequently for the f_{2r} and q_{2r}, it is now possible to return to the mainstream of the analysis with greater insight.

Case 1: $y'(o) = 0$

$$A = \frac{\mu \sum (fc + gs) + \sum r(fs - gc)}{2\left[\left\{\sum fc\right\}^2 - \mu\left\{\sum gs\right\}^2 - \left\{\sum fc\right\}\left\{\sum rgc\right\} - \left\{\sum gs\right\}\left\{\sum rfs\right\}\right]} \qquad (51)$$

Since the area of concern is when ions are transmitted it is reasonable to consider simplifications in the above expression which are valid only when A is relatively small. This will occur when the numerator is small and/or the numerator is large. The expression in the numerator can be simplified by noting that under the assumed

conditions $\mu << 1$. Then $g << f$. Then the numerator can be small only when the $\sum$ rfs term is small. Under these asemumptions and using Equation (50):

$$A_{22} \approx -\frac{q}{2} \sin \phi \tag{52}$$

Again with the denominator only the largest terms are considered giving:

$$D \approx \left[2 \quad 1 - \frac{q}{2} \cos \phi\right]^2 \tag{53}$$

This term will be at a maximum when $\phi = 180°$, however, it is clear that its affect upon the amplitude is not as severe as the numerator. Combining these last two expressions give:

$$Y_1 \approx -\frac{q \sin \phi}{4(1 - \frac{q}{2} \cos \phi)^2} \cdot y(o) \tag{54}$$

To complete the expression for y_{max} the term C must be evaluated. Again using Equations (50) and making the simplifying assumptions used above the result is

$$C \approx 1 + \frac{1}{2} q \tag{55}$$

Then for Case 1:

$$y_{max} \approx -\frac{q(1 + \frac{1}{2}q) \sin \phi}{4(1 - \frac{q}{2} \cos \phi)^2} \; y(o) \; e^{\mu\omega t/2} \tag{56}$$

There are limitations to the accuracy of Equation (56) which must be understood before it is applied. Note that according to this expression at $\phi = 0°$ and $180°$ $y_{max} = 0$. This is clearly not true since the other terms in Equation (51) will be non-zero. In the interest of completeness then for $\phi = 0$ and $180°$

$$Y_1 \approx \frac{\mu}{2(1 \mp \frac{q}{2})^2} \; y(o) \tag{57}$$

APPENDIX A

Comparing Equations (54) and (57), it follows that the latter expression is valid when $\mu >> \frac{1}{2}q\phi$.

Case 2: $y(o) = 0$

In this case $Y_1 = -(A_{12}/D)\, y'(o) = B\, y'(o)$

$$B = \frac{\sum(fc + gs)}{2\omega \left[\left\{\sum fc\right\}^2 - \mu\left\{\sum gs\right\}^2 - \left\{\sum fc\right\}\left\{\sum rqc\right\} - \left\{\sum gs\right\}\left\{\sum rfs\right\}\right]} \tag{58}$$

Again by a similar logic it is found that for Case 2:

$$Y_1 \approx \frac{1}{2(1 - \frac{q}{2}\cos\phi)} \frac{y'(o)}{\omega} \tag{59}$$

Comparing this expression to Equation (54) and (57) it is seen that Y_1 for Case 2 cannot ever be as small as for Case 1 for comparable values of $y(o)$ and $y'(o)/\omega$. The complete expression for y_{max} for Case 2 is:

$$y_{max} \approx \frac{(1 + \frac{1}{2}q)}{2(1 - \frac{q}{2}\cos\phi)} \frac{y'(o)}{\omega} e^{\mu\omega t/2} \tag{60}$$

According to this expression the worst case ϕ insofar as peak tails are concerned is $\phi = 180°$.

Case 3: $Ay(o) + By'(o) \approx 0$

APPENDIX A

For this case the interest is in that narrow range of initial phase where the initial velocity effects cancel the initial position effects. This will occur when:

$$\left(-\frac{q}{2}\sin\phi\right) y(o) + \left(1 - \frac{q}{2}\cos\phi\right)\frac{y'(o)}{\omega} = 0 \tag{61}$$

When this condition occurs:

$$Y_1 \approx \frac{\left(\mu \sum fc - \sum rgc\right) y(o) + \left(\sum gs\right)\ y'(o)/\omega}{2\left(\sum fc\right)^2} \tag{62}$$

From Equation (50) it is clear that the term in front of y(o) is approximately μ which leads to

$$Y_1 \approx \frac{\mu}{2}\left[\frac{y(o) - (q/2)\sin\phi\ y'(o)/\omega}{(1 - \frac{q}{2}\cos\phi)^2}\right] \tag{63}$$

where ϕ is evaluated using Equation (61). The corresponding expression for y_{max} is self-evident.

The analysis as conducted thus far gives theoretical expressions for the envelope of the y trajectory motion in the unstable region near the y stability boundary. These expressions offer insight into the factors which control these trajectories. It now remains to examine the effect upon peak tails.

Tail Analysis

In order to analyze the tails on the mass filter peaks utilizing the results of the preceding section it is necessary to relate the stability parameter μ to quantities which are more meaningful. Evaluating the case r = 0 in Equation (42) and making appropriate substitutions from Equation (40) and (50) the following is obtained.

$$\begin{aligned} c_o &= (c_2 + c_{-2})(A_o - i\,B_o) \\ &\approx -\frac{q^2}{2(a + \mu^2)} \approx 1 \end{aligned} \tag{64}$$

where the complex conjugate properties of c_2 and c_{-2}, and the normalization of c_o have been employed. Note that for $\mu = 0$, the results are

$$a_o \approx -\frac{1}{2} q^2 \tag{65}$$

which agrees with the expression given by McLachlin[3]. Since Equation (65) is only approximate it is necessary to work in terms of delta values for a and q rather than a and q directly. Therefore, let

$$a = a_o + \Delta a \qquad q = q_o + \Delta q \tag{66}$$

and assume that operation is on a scan line as is normally done, i.e.,

$$a = -sq \tag{67}$$

where the negative sign indicates operation in the fourth quadrant of the full stability diagram. Substituting these expressions into Equation (64) and making use of the fact that $\mu = 0$ (a_o, q_o) gives:

$$\mu \approx \left[-\Delta a - q\Delta q - \frac{1}{2} \Delta q)^2\right]^{1/2}$$

$$\approx \left[-\Delta a - q\Delta q\right]^{1/2}$$

where the second order term in Δq is dropped. Then making use of the constraint implied by Equation (67)

$$\mu \approx \left[(s - q)\ \Delta q\right]^{1/2}$$

$$\approx \left[(a - q)\ \frac{\Delta q}{q}\right]^{1/2}$$

Since $a < 0$ and $\Delta q < 0$ for the case at hand:

$$\mu \approx \left[(a + q)\ \frac{\Delta q}{q}\right]^{1/2} \tag{68}$$

[3] Ibid. Page 16

where Δq is now taken as positive. The values for a and q can be taken as the values at the apex of the stability diagram, i.e., $a = 0.237$, $q = 0.706$. Furthermore, from the definition of q in terms of quadrupole parameters, i.e.,

$$q = \frac{4\ e\ V_{ac}}{m r_o^2 \omega^2}$$

it follows that

$$\frac{\Delta q}{q} = \frac{\Delta m}{m}$$

thus

$$\mu \approx 0.97 \left(\frac{\Delta m}{m}\right)^{1/2}$$

or more approximately

$$\mu \approx \left(\frac{\Delta m}{m}\right)^{1/2}$$

Therefore $\frac{\Delta m}{m} = 0.01$, $\mu = 0.1$ which defines the conditions under which the analysis in the preceding section is valid. The advantage of expressing μ in terms of $\Delta m/m$ is that now the magnitude of a peak tail can be determined at a distance from the stability boundary which is measured in peak widths. Suppose that a specification is given in terms of a allowable crosstalk one mass unit from the center of a mass peak with a basic resolving power of 100, i.e., suppose that without tails the resolving power would be 100. Then the value of $\Delta m/m$ to be used would be 1/200. See the figure below:

APPENDIX A

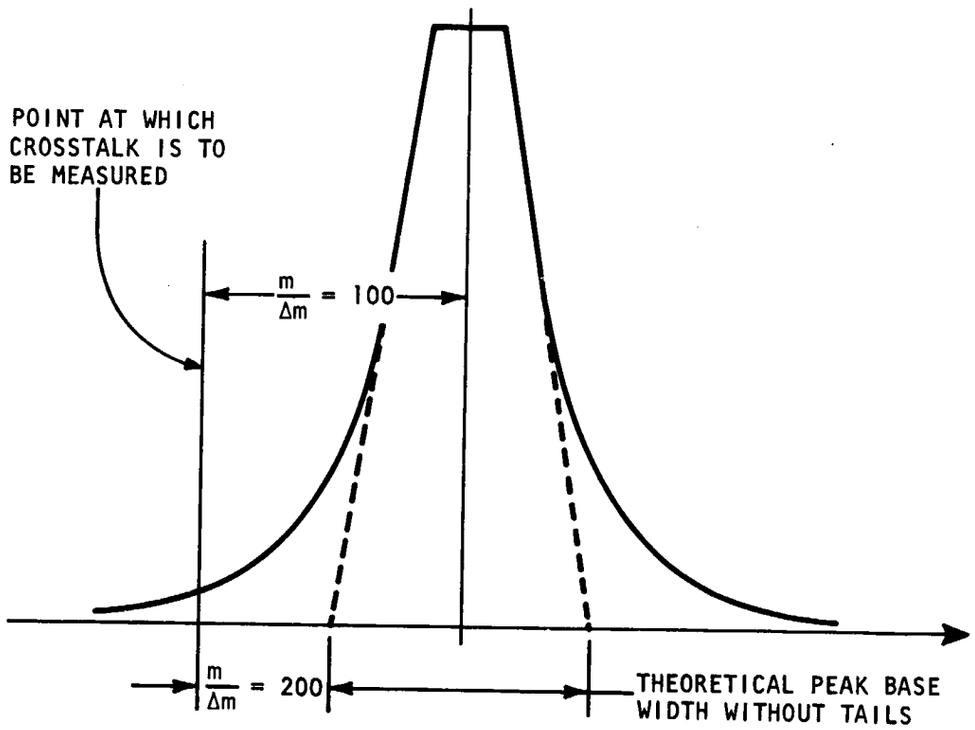

It is probably more meaningful to let

$$\mu = \left(t \frac{\Delta m}{m}\right) 1/2 \tag{69}$$

where t is a number indicating the fraction of the fundamental or theoretical peak base width which is included as part of the total peak for the purposes of computing the size of the peak tail.

As an illustration of how a complete analysis might go the special case $y'(o) = 0$ is considered in the following paragraphs since the peak tail size is dependent upon the transmission of ions, and since this is determined by the ion amplitude relative to r_o, the rod spacing parameter, it is necessary to write a transmission criterion using Equation (58):

$$r_o > \left| \frac{- q(1 + \frac{1}{2} q) \sin \phi}{4(1 - \frac{q}{2} \cos \phi)^2} \; y(o) \; e^{\mu \omega t/2} \right| \tag{70}$$

APPENDIX A

Substituting Equation (69) along with $n = \omega t/2\pi$ and evaluating the terms involving q gives:

$$r_o > \left| \frac{-0.24 \sin \phi}{(1 - 0.35 \cos \phi)^2} \; y(o) \; e^{\pi n (t\Delta m/m)^{1/2}} \right| \tag{71}$$

let $\eta = y(o)/r_o$ then

$$\frac{(1 - 0.35 \cos \phi)^2}{0.24 \, \eta |\sin \phi|} > \exp \left[\pi n (t\Delta m/m)^{1/2} \right] \tag{72}$$

Let ϕ_1 and ϕ_2 be the transmission limits over which Equation (72) is satisfied for any given set of parameters η, n, t, and $\Delta m/m$. Then, if $\Delta\phi = \phi_2 - \phi_1$, (always positive), the fraction of ions transmitted for any set of parameters will be $\Delta\phi/2\pi$. The total fraction of ions transmitted over all η is:

$$\Theta = 2\pi\eta_o \int_o^{\eta_o} \Delta\phi(\eta) d\eta \tag{73}$$

Where η_o is the limit on η represented by the ion entrance aperture and the width of the entrance aperture is assumed to be independent of y, i.e., a square or rectangular aperture is assumed. The parameter θ is called the transmission efficiency.

From this point it is very difficult to proceed analytically without resorting to numerical techniques. If the $\cos \phi$ term in Equation (72) is ignored and the resulting expression is substituted into Equation (73) the result is:

$$\Theta \approx \frac{2}{\pi} \sin^{-1}\left(\frac{\eta_1}{\eta_o}\right) + \frac{2}{\pi} \frac{\eta_1}{\eta_o} \log_e \left(\frac{\eta_o}{\eta_1} + \sqrt{\left(\frac{\eta_o}{\eta_1}\right)^2 - 1} \right)$$

where

$$\eta_1 = \frac{1}{0.24 \exp \left[\pi n (t\Delta m/m)^{1/2} \right]}$$

and has the physical significance that for $\eta < \eta_1$ all phase angles are transmitted. Note that for $\eta_1 = \eta_o$, $\theta = 1$ as it should. The expression for θ can be written:

$$\theta = f(\eta_1/\eta_o)$$

Taking the inverse of this function:

$$\frac{\eta}{\eta_o} = f^{-1}(\theta)$$

Substituting for η_1 and solving for n yields:

$$n = \left[\frac{1}{\pi t^{1/2}} \log_e \left(\frac{1}{0.24\ \eta_1\ f^{-1}(\theta)}\right)\right] \left(\frac{m}{\Delta m}\right)^{1/2}$$

$$n = K\left(\frac{m}{\Delta m}\right)^{1/2}$$

which is the same form as the well known empirical expression of von Zahm[4]:

$$n = 3.5\left(\frac{m}{\Delta m}\right)^{1/2}$$

It is difficult to determine if the expression which was derived will give a number that is close to this. The following numerical example is given:

$$\theta = 0.25 \Rightarrow f^{-1}(\theta) \simeq 0.1$$

$$\eta_o = 0.1$$

$$t = 0.5$$

[4]DAS Electrische Massen Filter ALS Massen Spektrometer und Isotopentrenner, W. Paul, H.P. Reinhard, und V. von Zahn, Zeitschrift für Physik, 1958.

and the result is:

$$n \approx 2.7\ (m/\Delta m)^{1/2}$$

the expression appears to be of the correct order of magnitude.

The numerical results derived above are not of great significance, but the deriviation does emphasize that the often quoted expression of von Zahm is nothing more than an empirical equation which expresses the results obtained on a particular instrument (η_o) under particular criteria (t, θ). Therefore, it is not reasonable to extend these results to other instruments, and a more complete analysis is required.

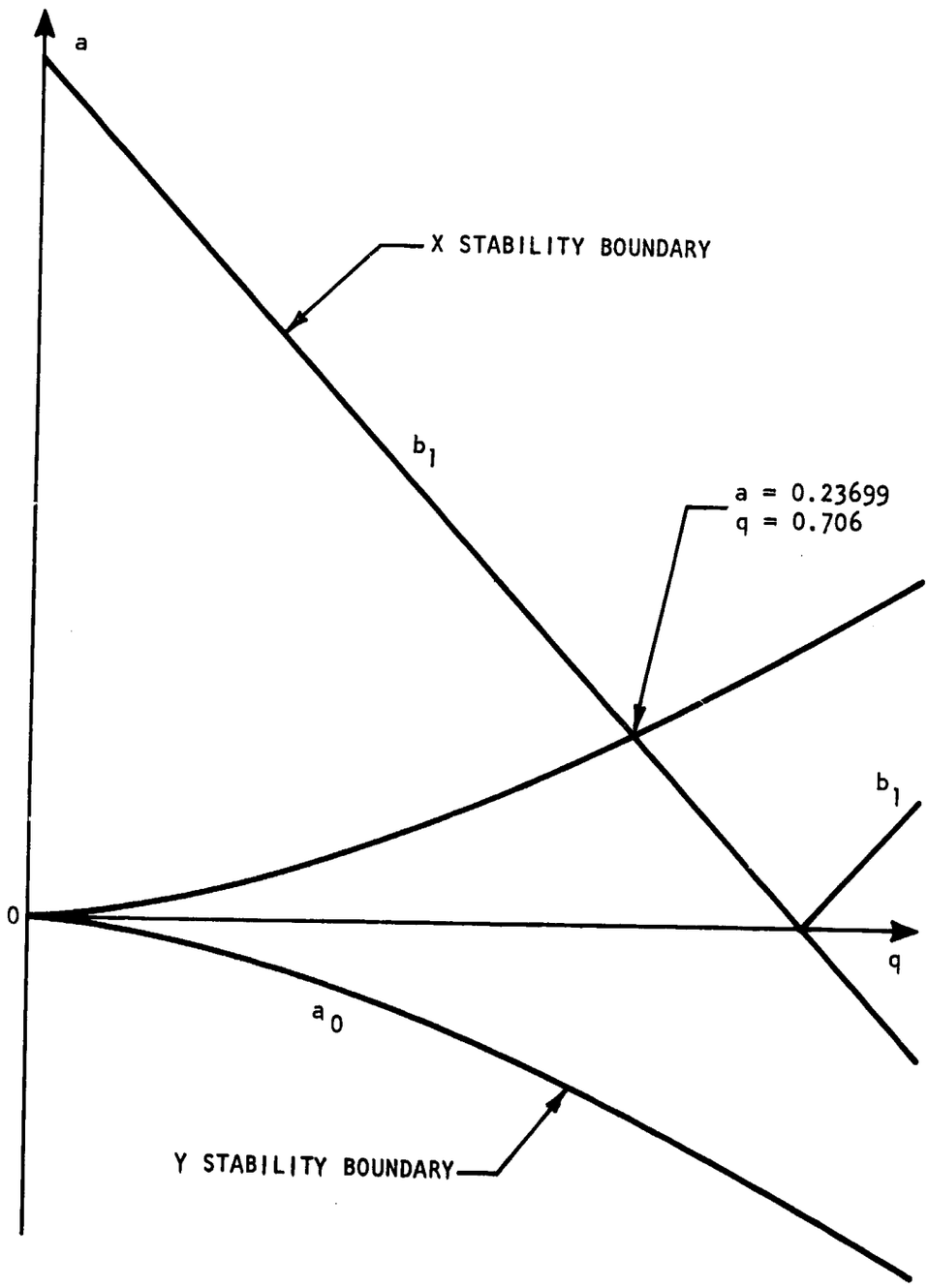

FIGURE 1. Mathieu D.E. Stability Diagram

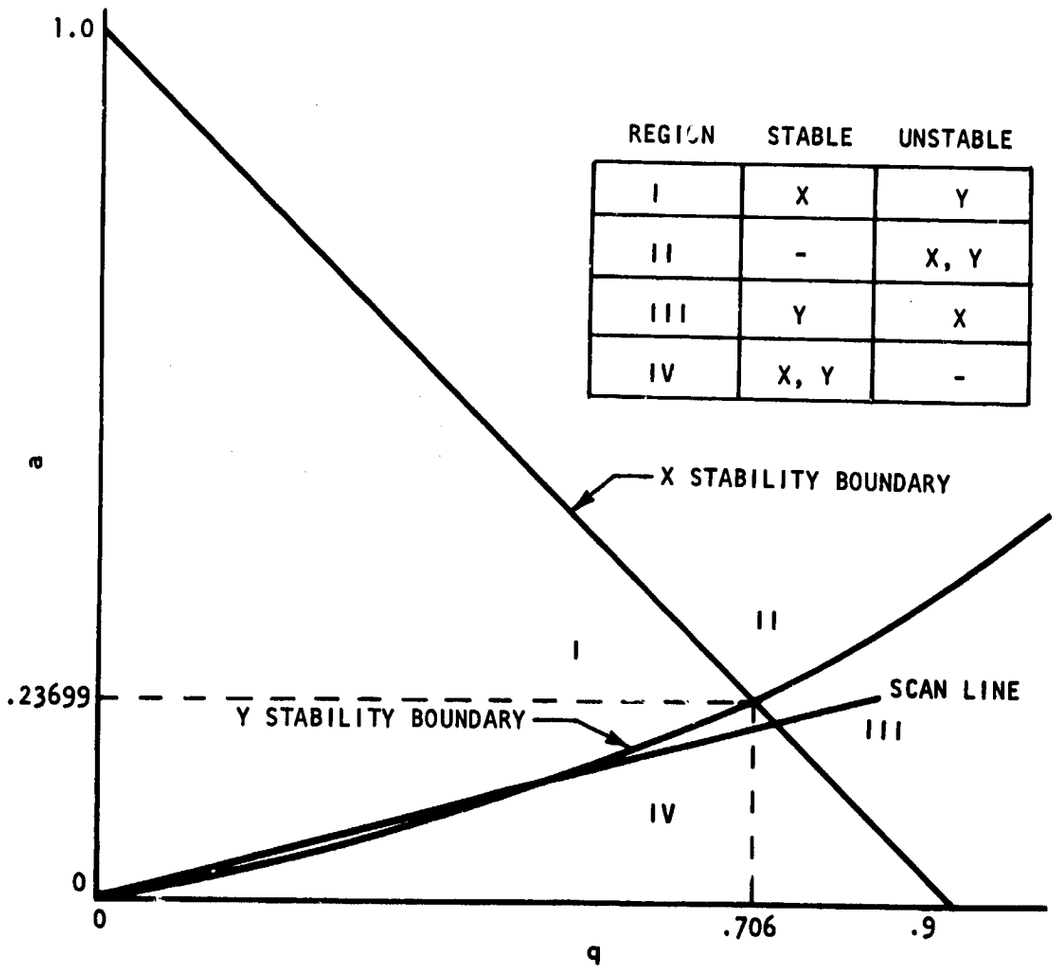

FIGURE 2. Typical Stability Diagram

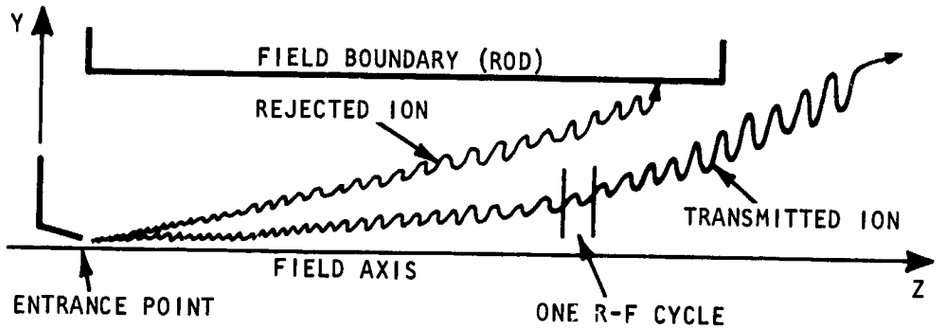

FIGURE 3. Transmission of Unstable Ions in a Quadrupole Field

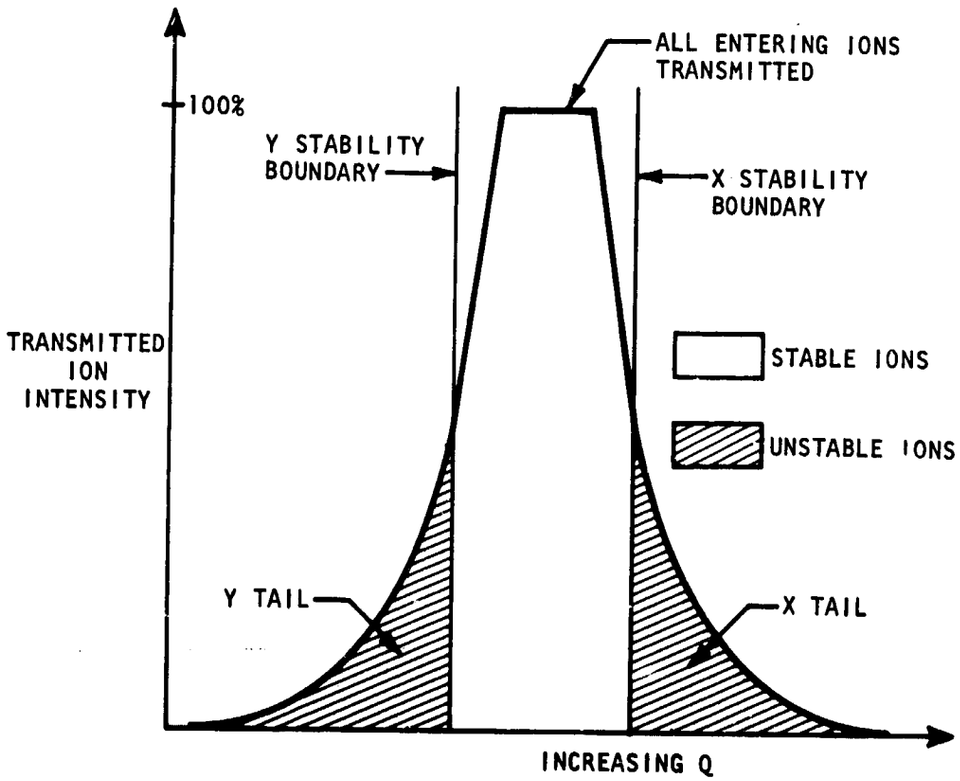

FIGURE 4. Peak Tails

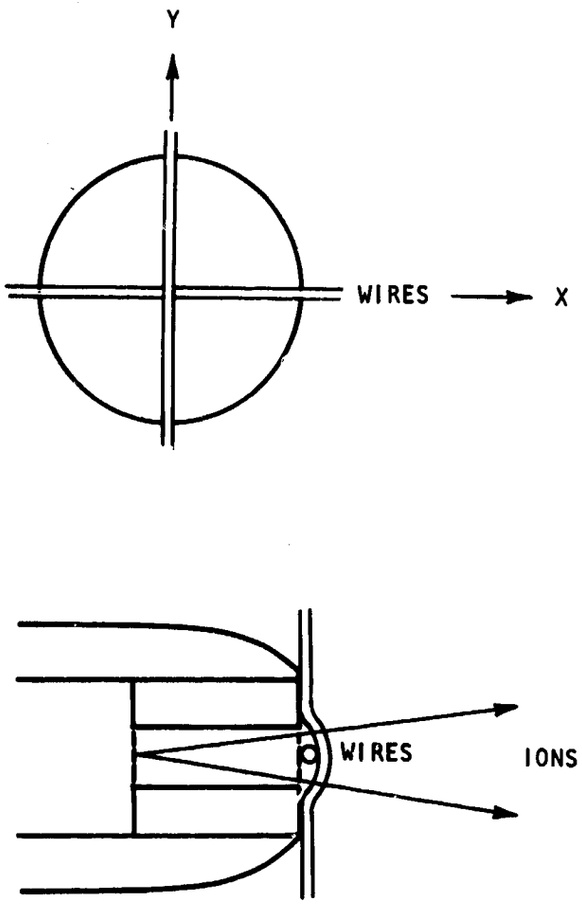

FIGURE 5. η-Mask on Nozzle Exit

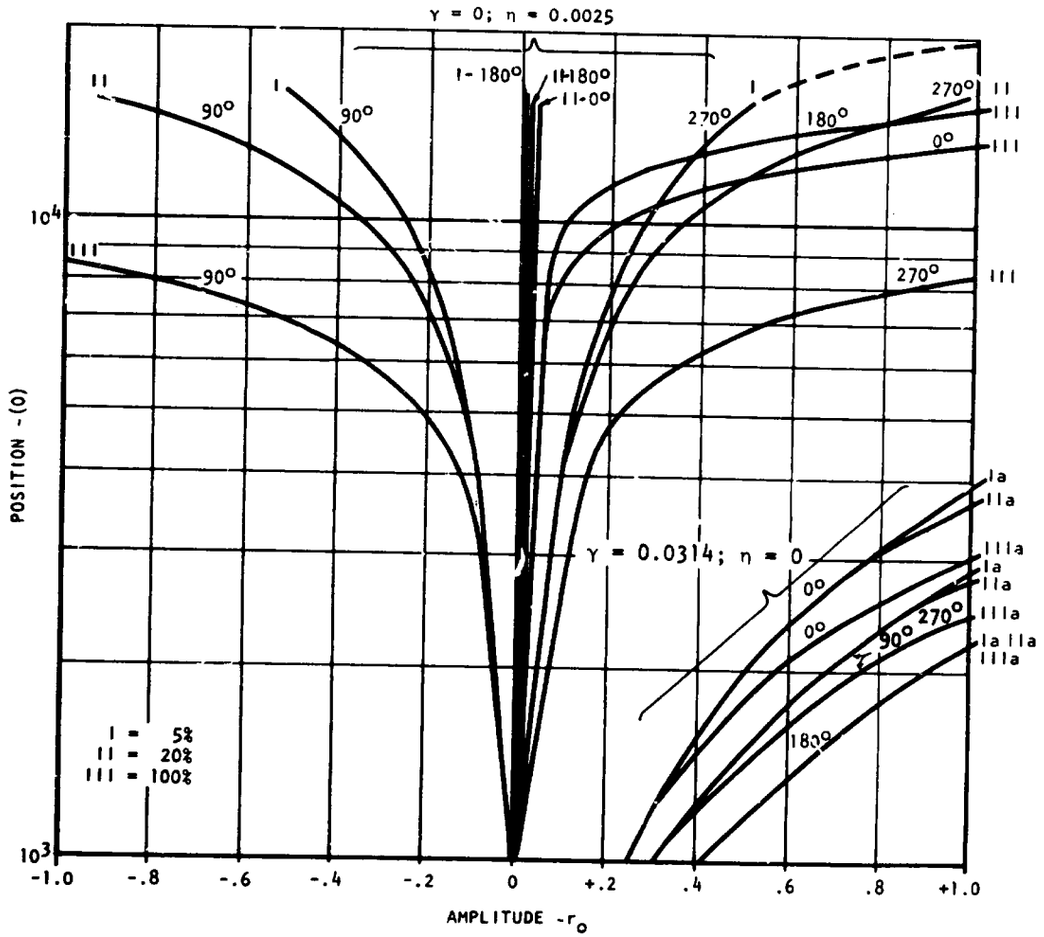

FIGURE 6. Ion Trajectories (γ = 0 and 0.0314; η = 0 and 0.0025)

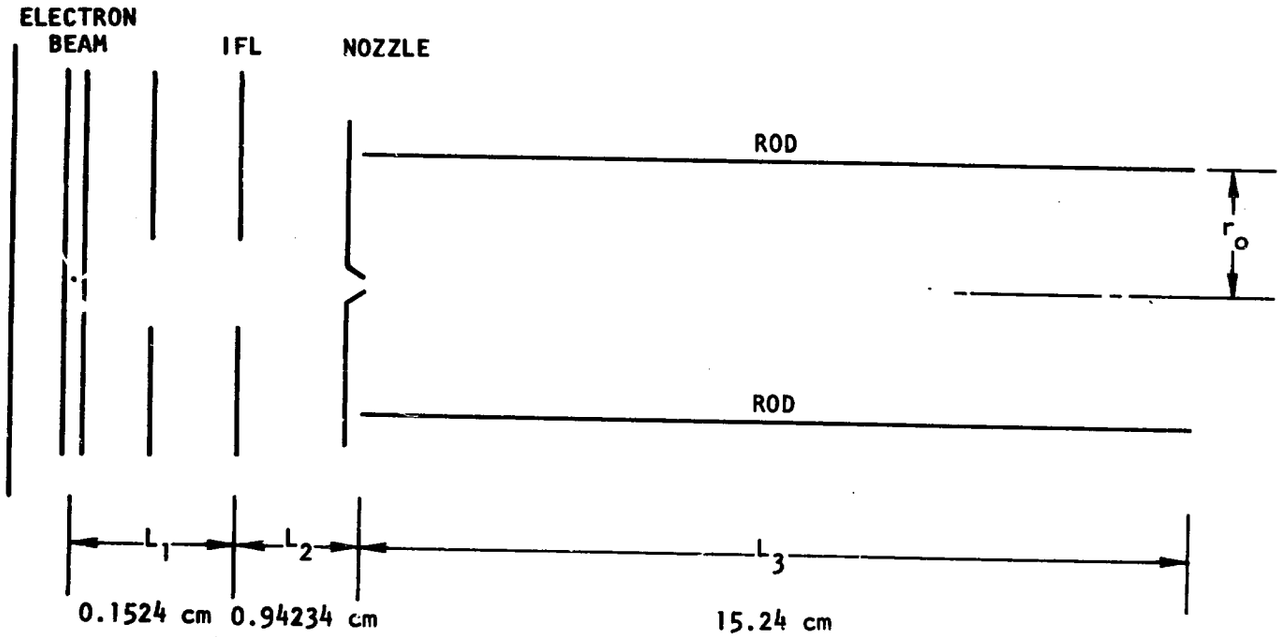

FIGURE 7. Geometry of Quadrupole

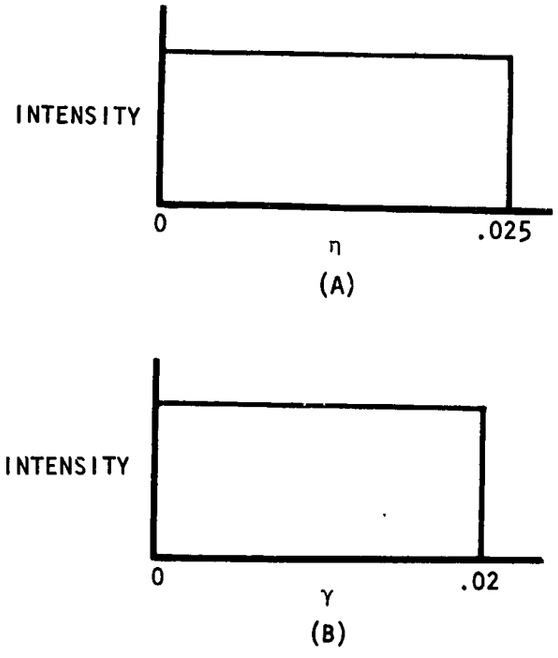

FIGURE 8. Intensity Distribution

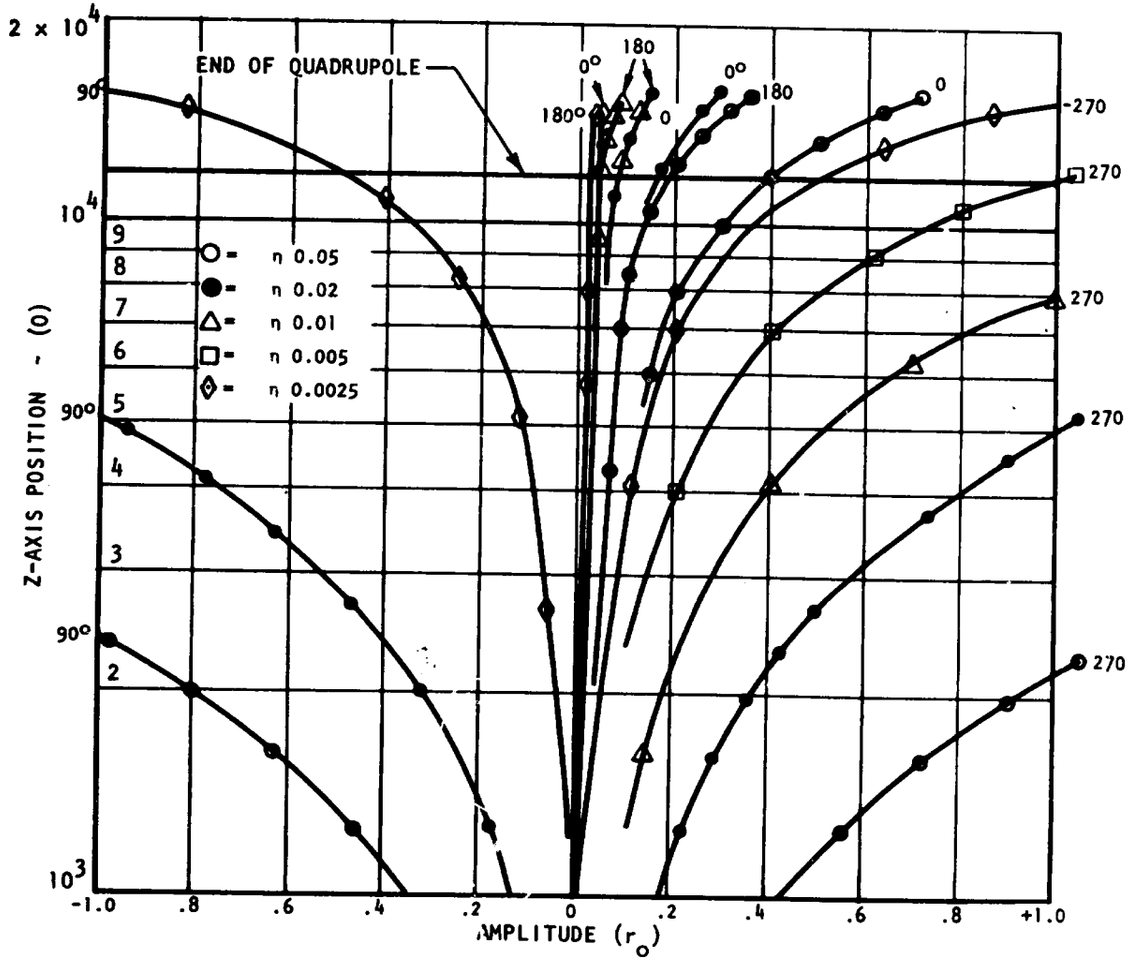

FIGURE 9. Ion Trajectories for Various η Values

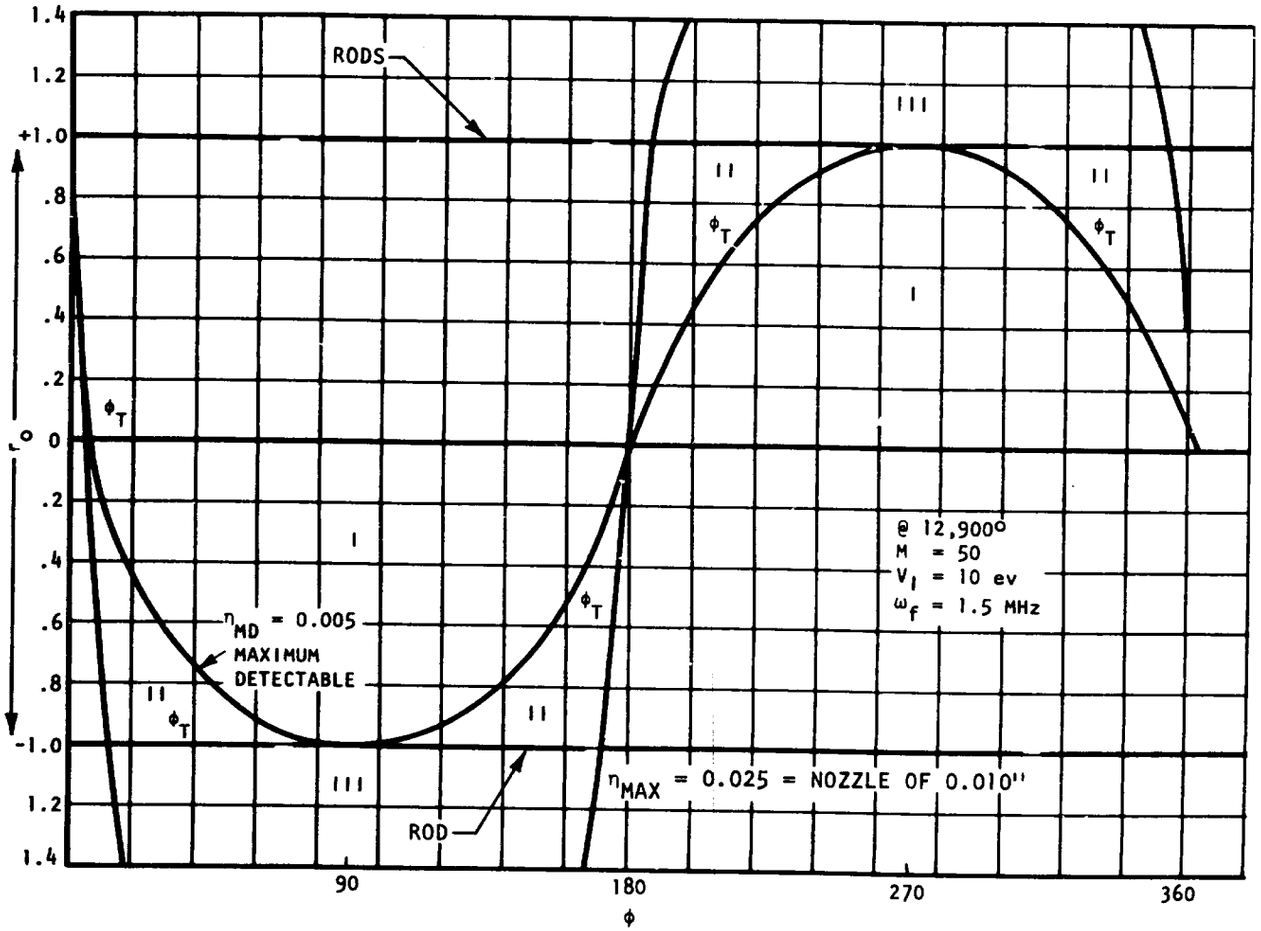

FIGURE 10. Unstable Ion Transmission, Δq = 20%, γ = 0

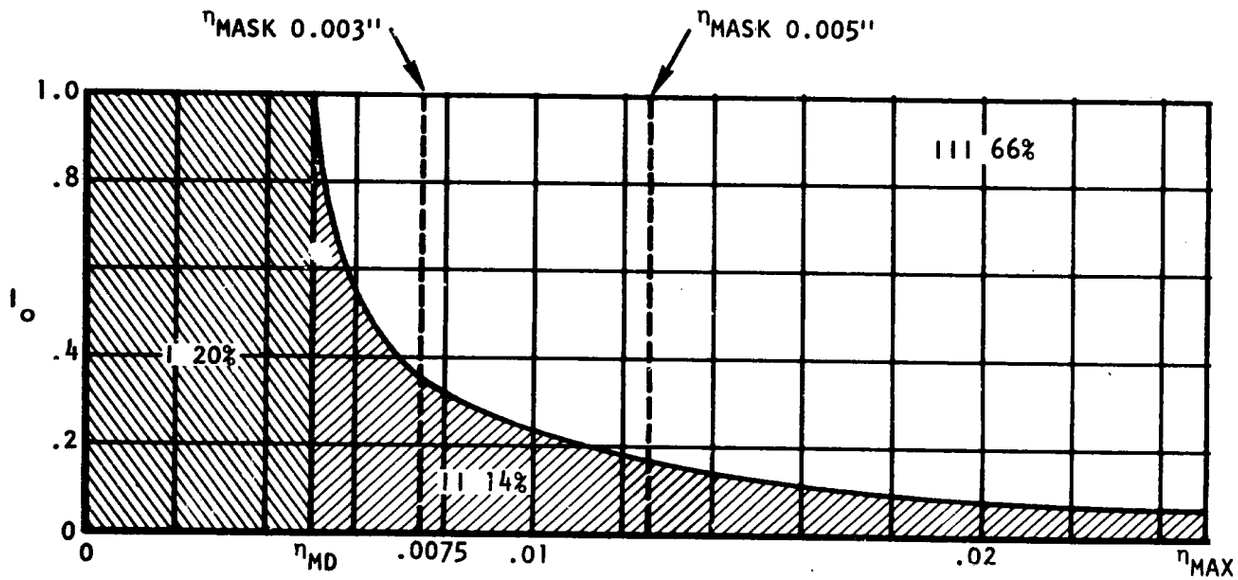

TOTAL TAIL INTENSITY
-34% WITHOUT MASK
- 9% WITH 0.003" MASK
- 5% WITH 0.005" MASK

FIGURE 11. Intensity of Tail (Approximate) With and Without Masking Δq = 20%

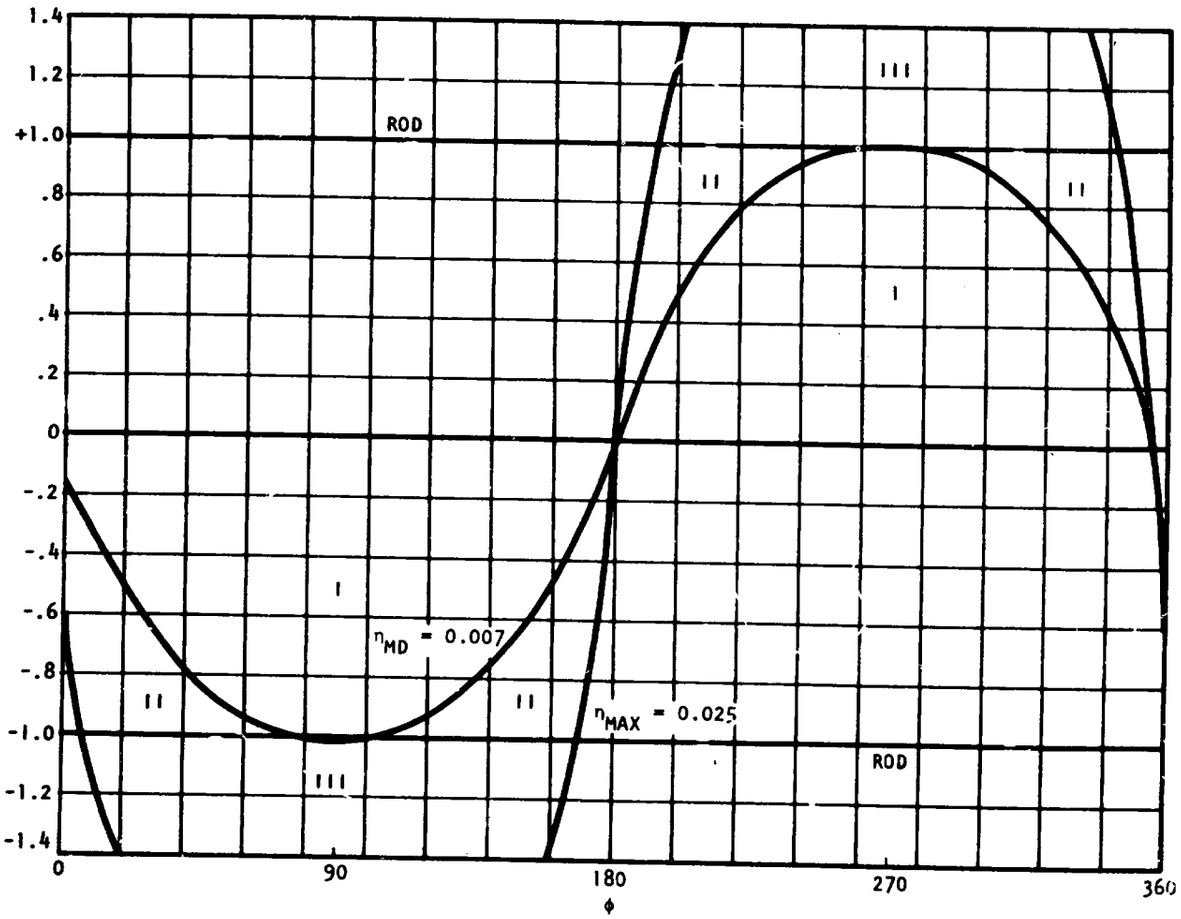

FIGURE 12. Unstable Ion Transmission, Δq = 5%

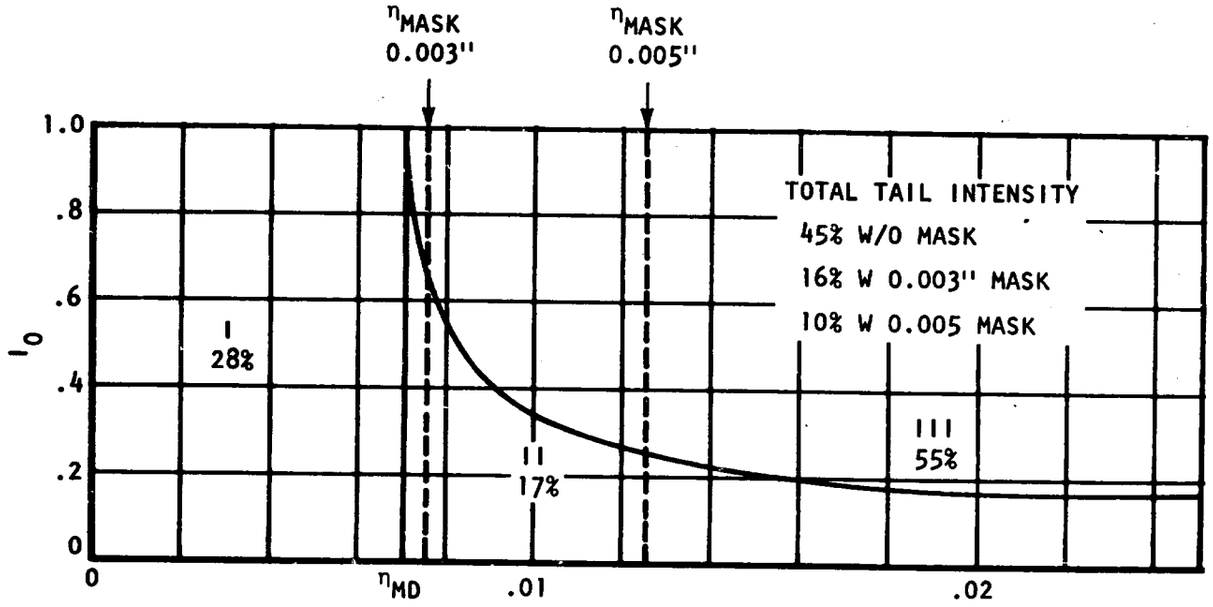

FIGURE 13. Intensity of Tail (Approximate) With and Without Masking, Δq = 5%

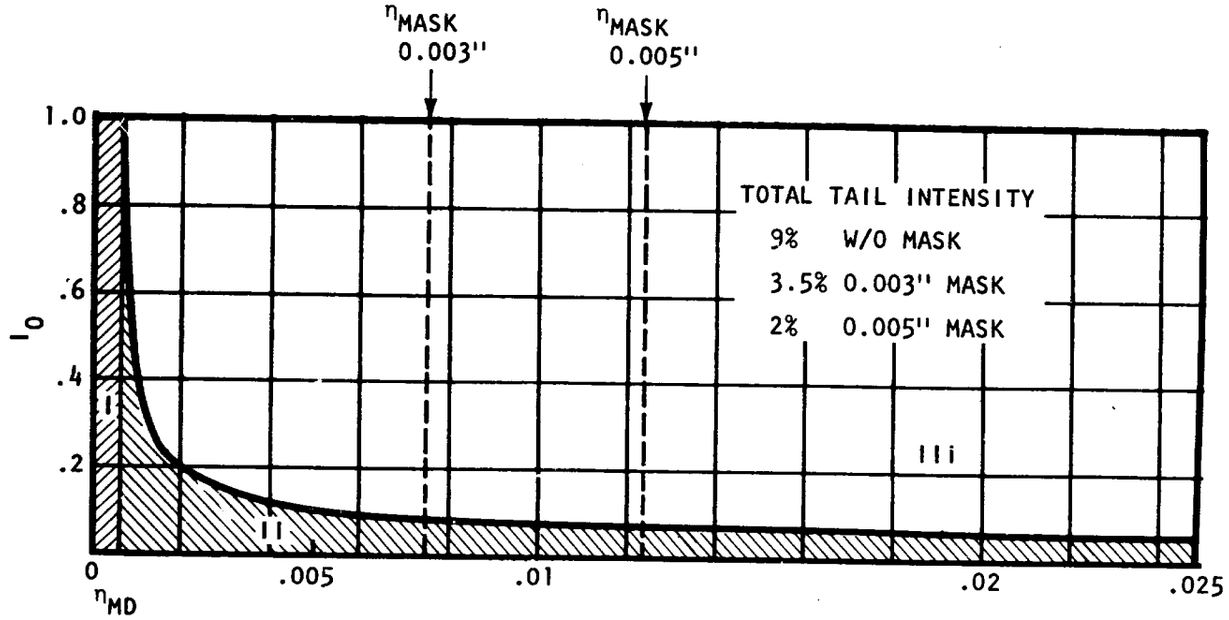

FIGURE 14. Tail Intensity at Δq = 100%

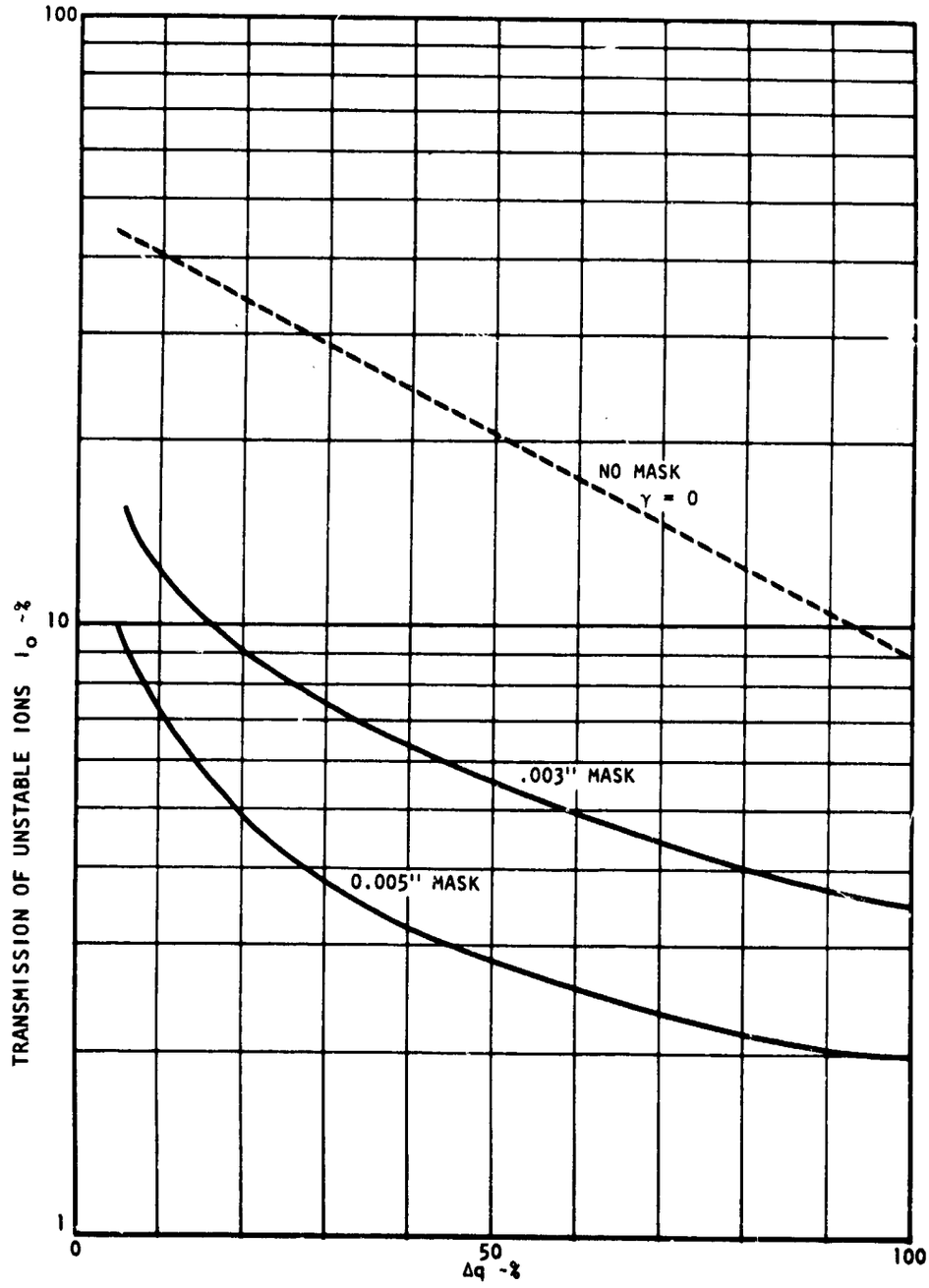

FIGURE 15. Tail Amplitude vs q, = 0

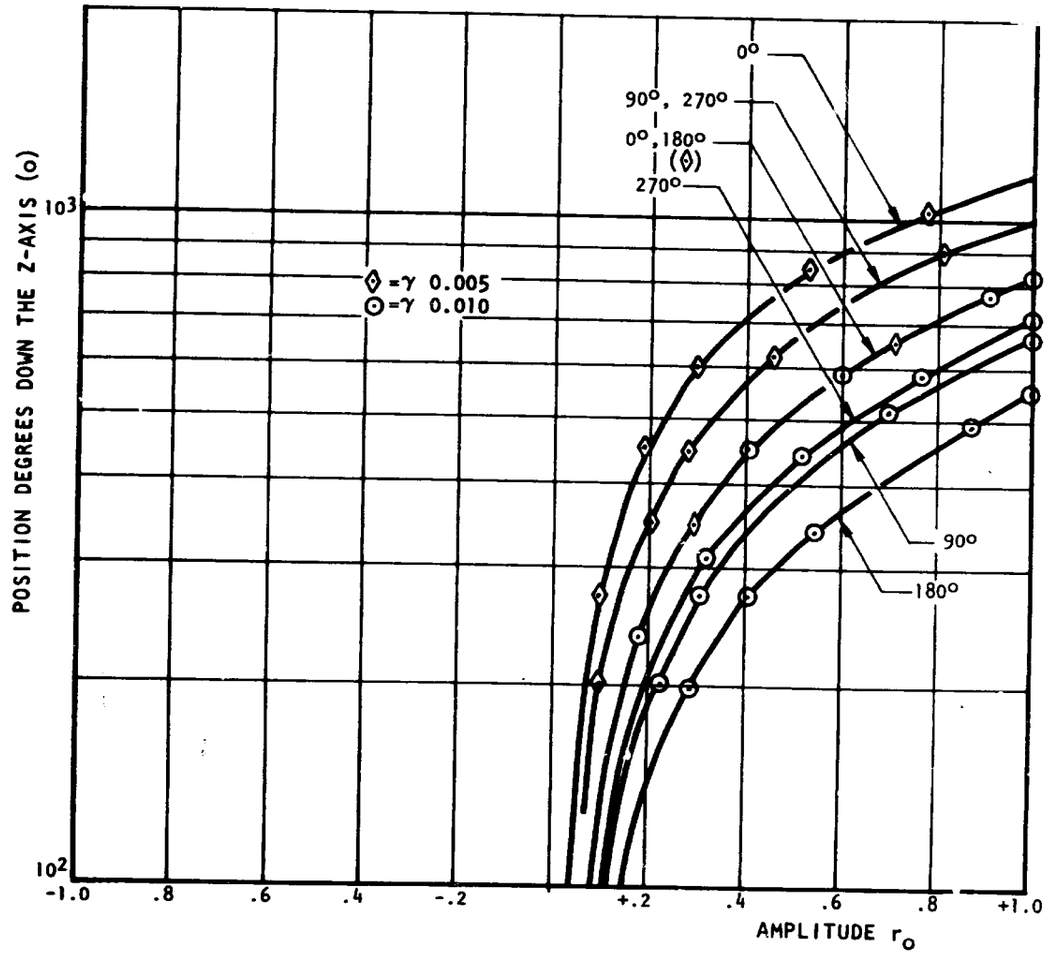

FIGURE 16. Ion Amplitude, Δq = 20%; $M/\Delta M$ = 100

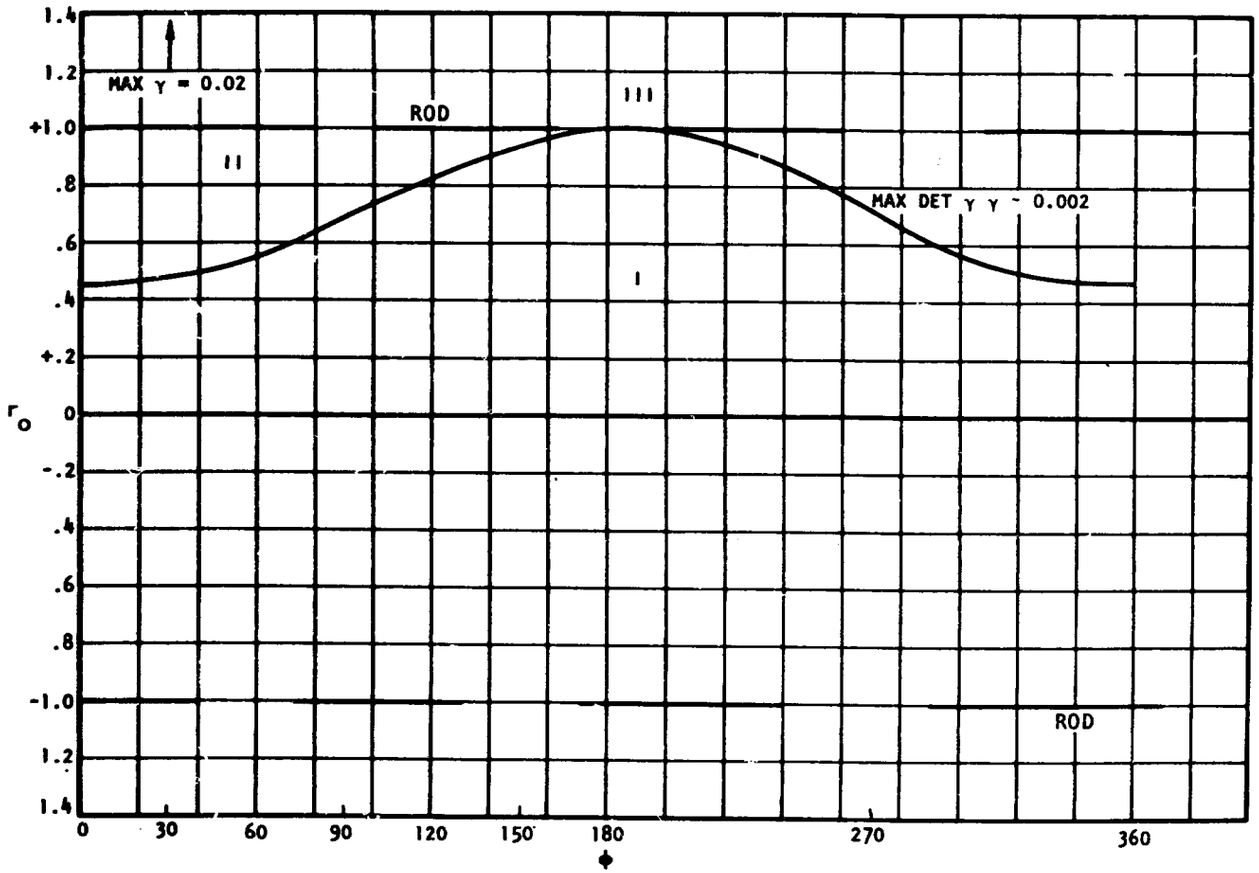

FIGURE 17. Amplitude as a Function of Phase, Δq = 20%; η = 0

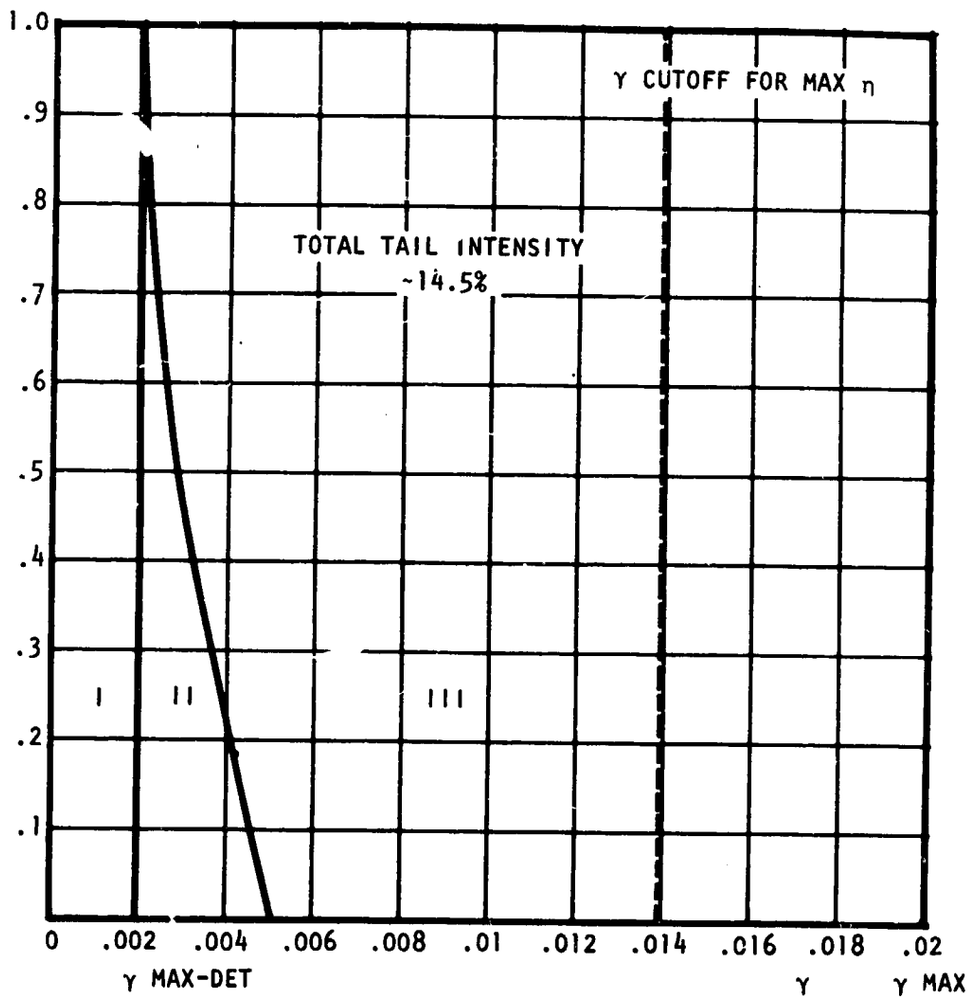

FIGURE 18. Total γ Tail Intensity, Δq = 20%

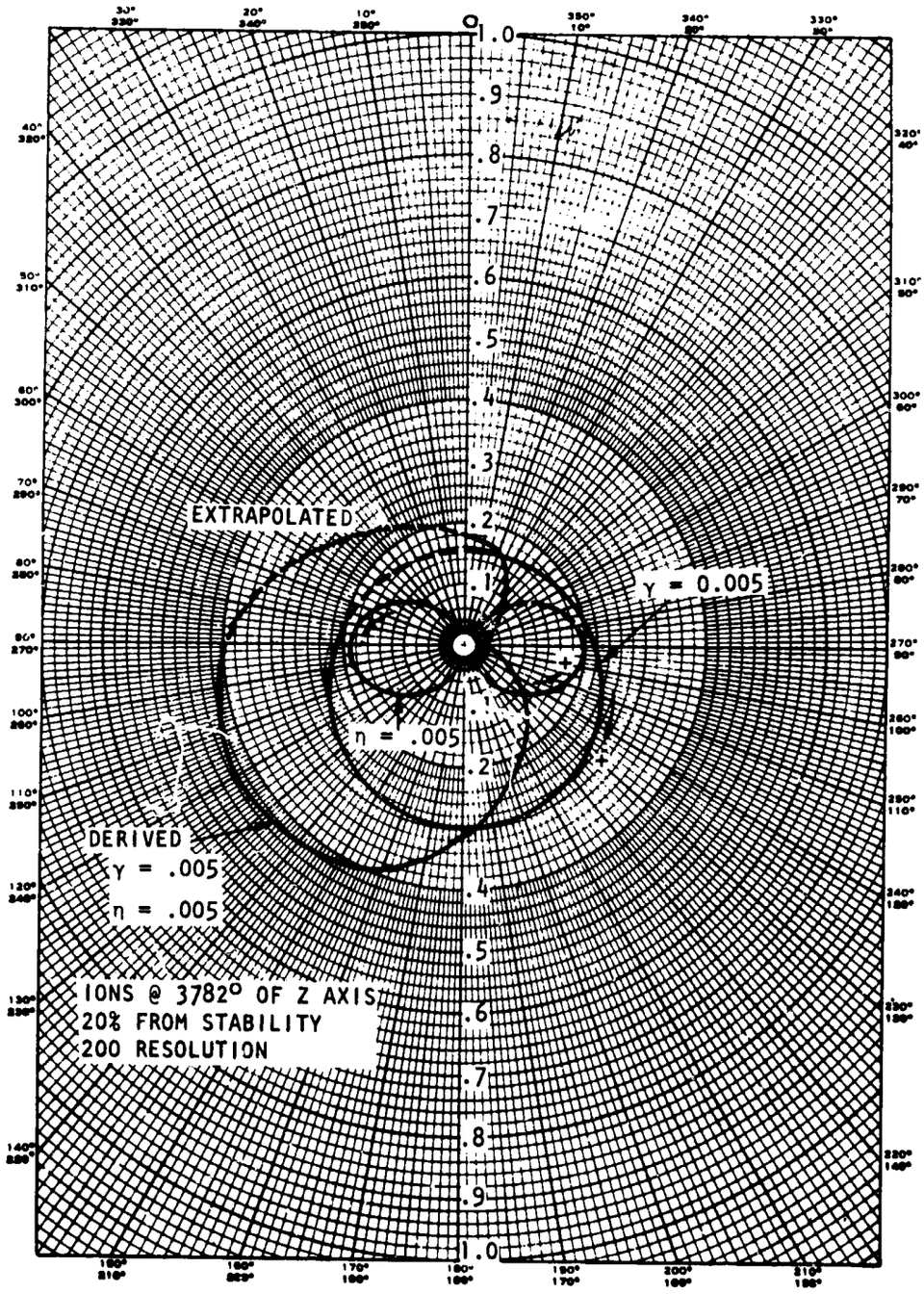

FIGURE 19. Ion Amplitude vs Initial Phase

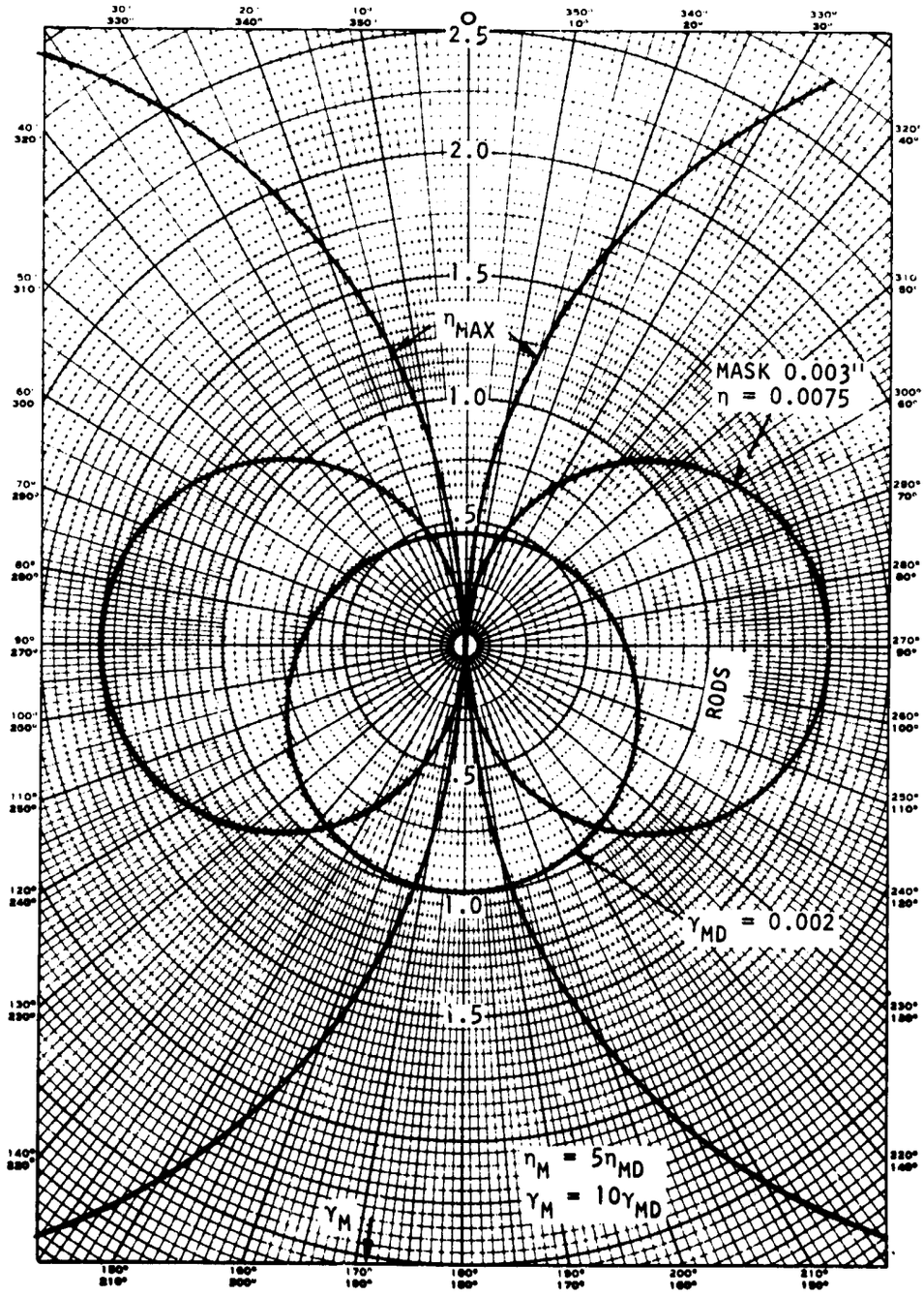

FIGURE 20. Ion Amplitude vs η or γ

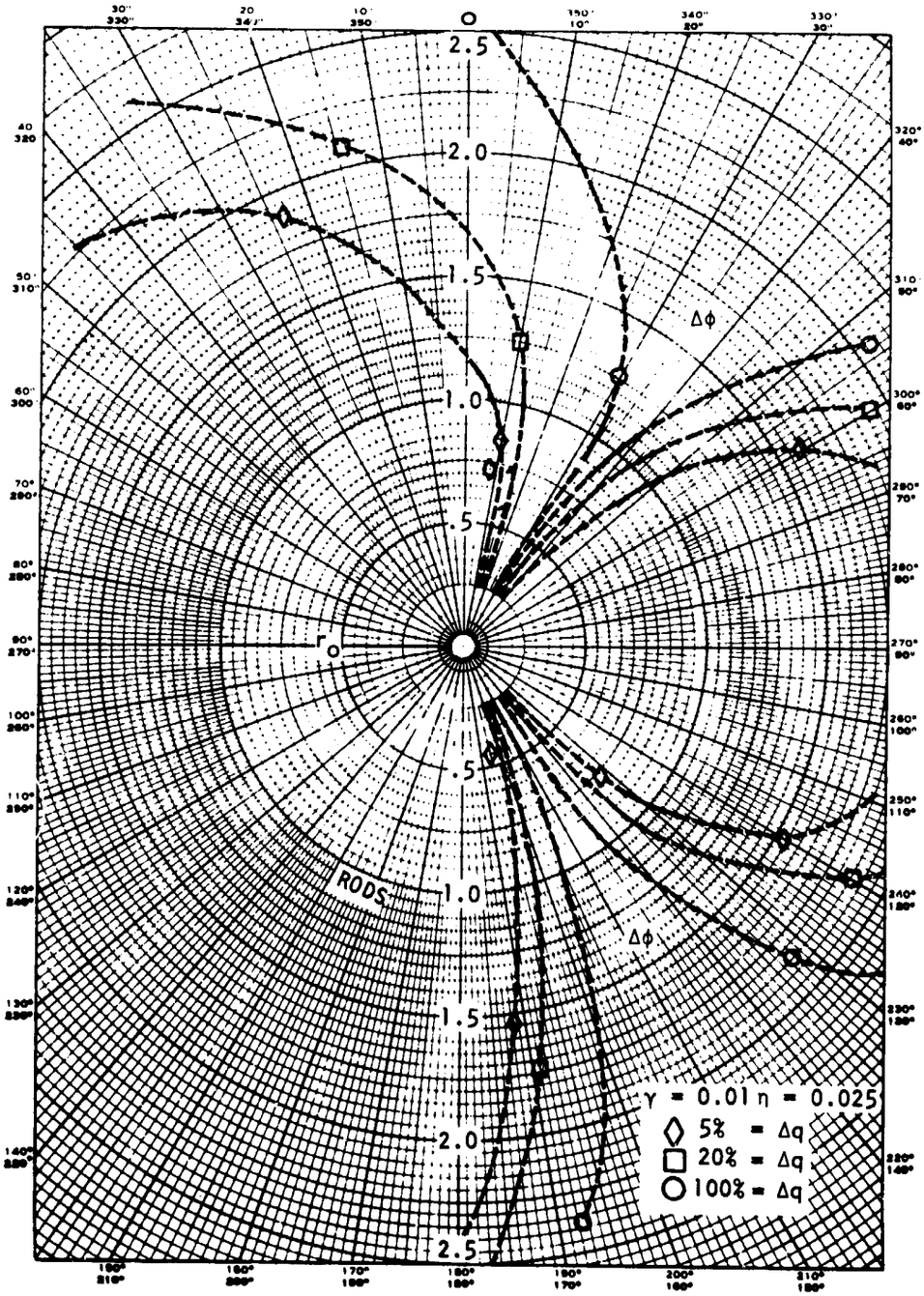

FIGURE 21. Bandwidth of Transmission

Φ	η	γ	A
0.	.0235	.004	1.024
6.	.0215	.006	1.027
13.	.0215	.008	1.027
13.	.0235	.000	-1.021
17.	.0175	.000	-1.020
19.	.0235	.002	-1.028
19.	.0235	.010	1.024
23.	.0195	.002	-1.031
30.	.0115	.008	1.022
31.	.0095	.000	-1.019
39.	.0255	.008	-1.029
42.	.0115	.002	-1.026
43.	.0155	.004	-1.030
44.	.0095	.008	1.026
44.	.0235	.008	-1.030
45.	.0135	.010	1.025
51.	.0215	.008	-1.028
52.	.0175	.006	-1.029
56.	.0095	.002	-1.029
56.	.0235	.016	1.031
60.	.0195	.014	1.025
63.	.0195	.008	-1.025
69.	.0155	.006	-1.022
76.	.0255	.012	-1.024
77.	.0255	.012	-1.028
82.	.0255	.012	-1.029
83.	.0255	.012	-1.024
86.	.0195	.014	1.021
92.	.0235	.016	1.029
94.	.0095	.008	1.021
94.	.0155	.006	-1.023

FIGURE 22. Typical $\Delta\phi$ Data (Sheet 1 of 2)

Φ	η	γ	A
99.	.0135	.010	1.023
99.	.0195	.008	-1.021
112.	.0255	.010	-1.023
114.	.0155	.010	1.025
115.	.0095	.002	-1.026
115.	.0115	.008	1.022
117.	.0075	.006	1.022
130.	.0115	.002	-1.030
130.	.0195	.010	1.027
133.	.0175	.004	-1.023
134.	.0155	.008	1.022
135.	.0215	.010	1.020
146.	.0235	.004	-1.027
149.	.0095	.000	-1.020
150.	.0235	.008	1.019
152.	.0195	.002	-1.029
154.	.0175	.006	1.026
158.	.0095	.004	1.020
163.	.0175	.000	-1.020
166.	.0155	.004	1.024
167.	.0235	.000	-1.021
180	.0235	.002	1.024

FIGURE 22. Typical Δϕ Data (Sheet 2 of 2)

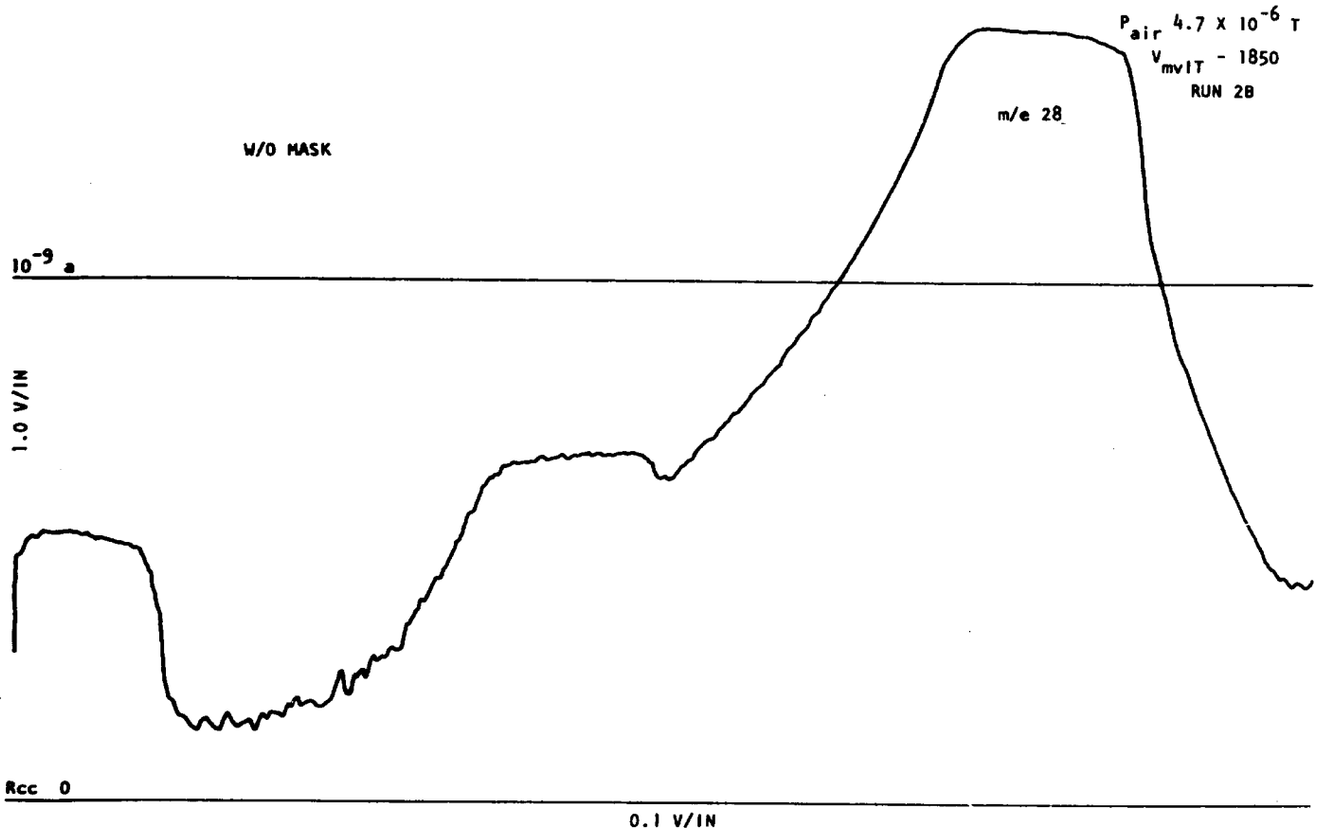

FIGURE 23. Peak Shape Without Mask

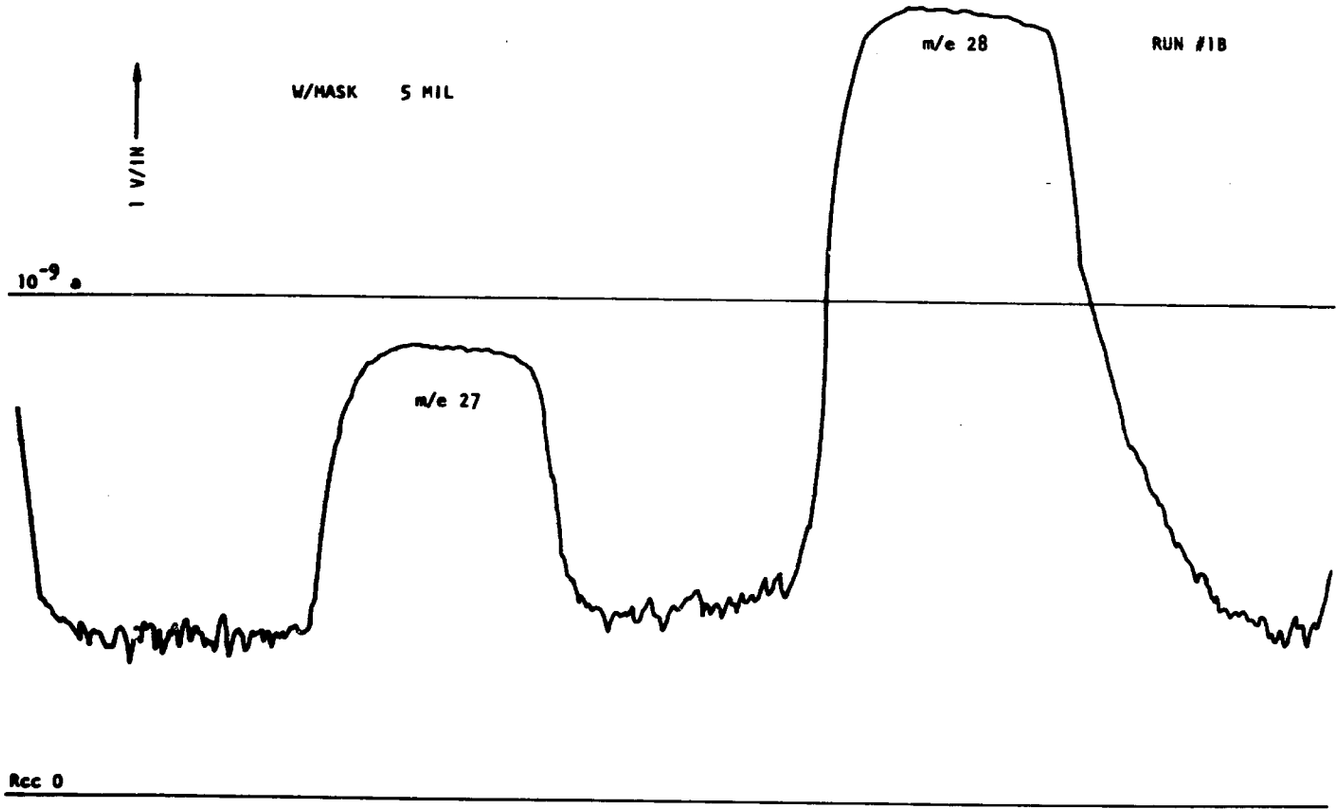

FIGURE 24. Peak Shape With 0.005 Inch Mask on Y-Axis

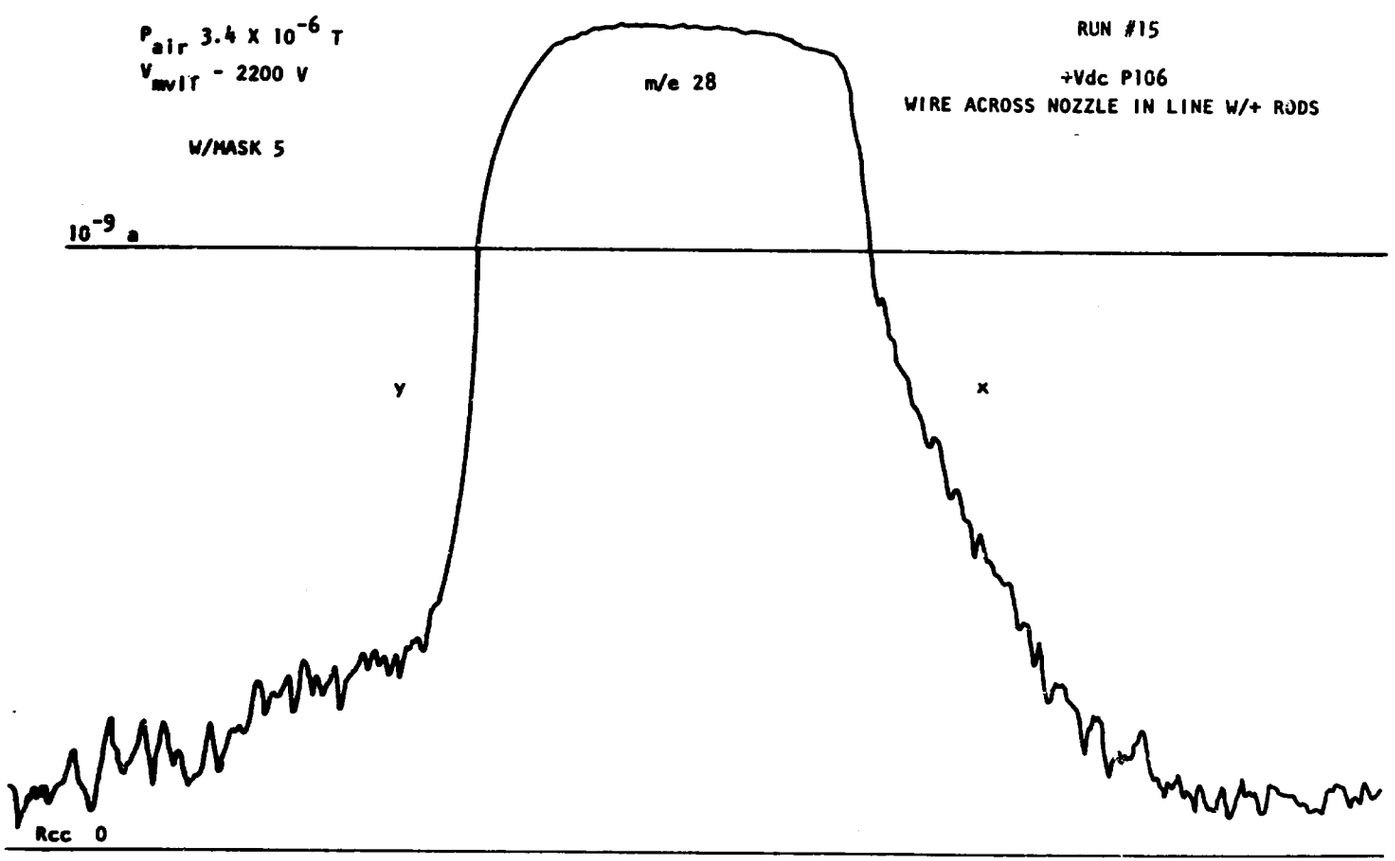

FIGURE 25. Mask on Y-Axis

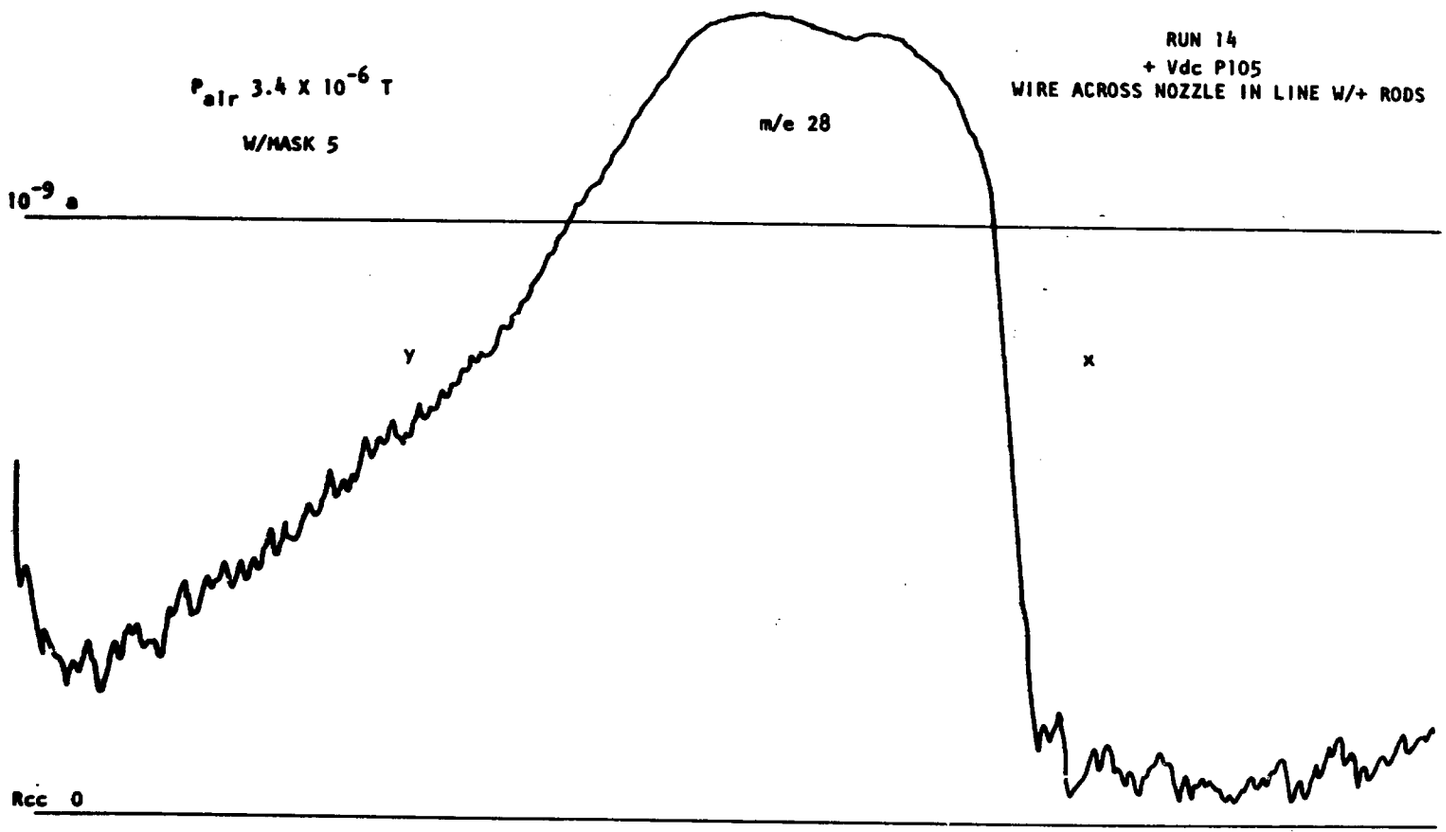

FIGURE 26. Mask on X-Axis

FIGURE 27. Peak Shape With 0.003 Inch Cross Mask

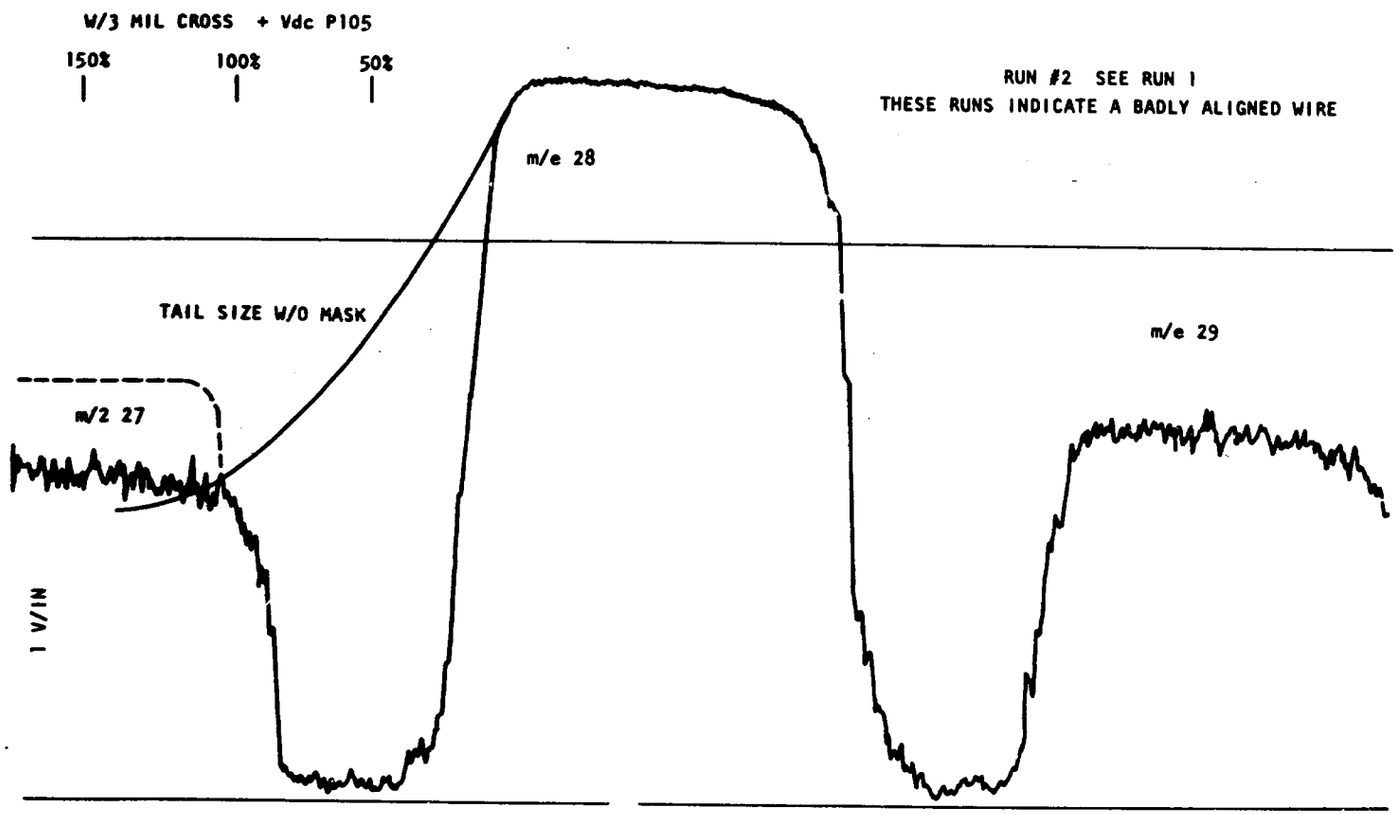

FIGURE 28. Peak Shape With 0.003 Inch Cross Mask
(Rod DC Potential Reversed)

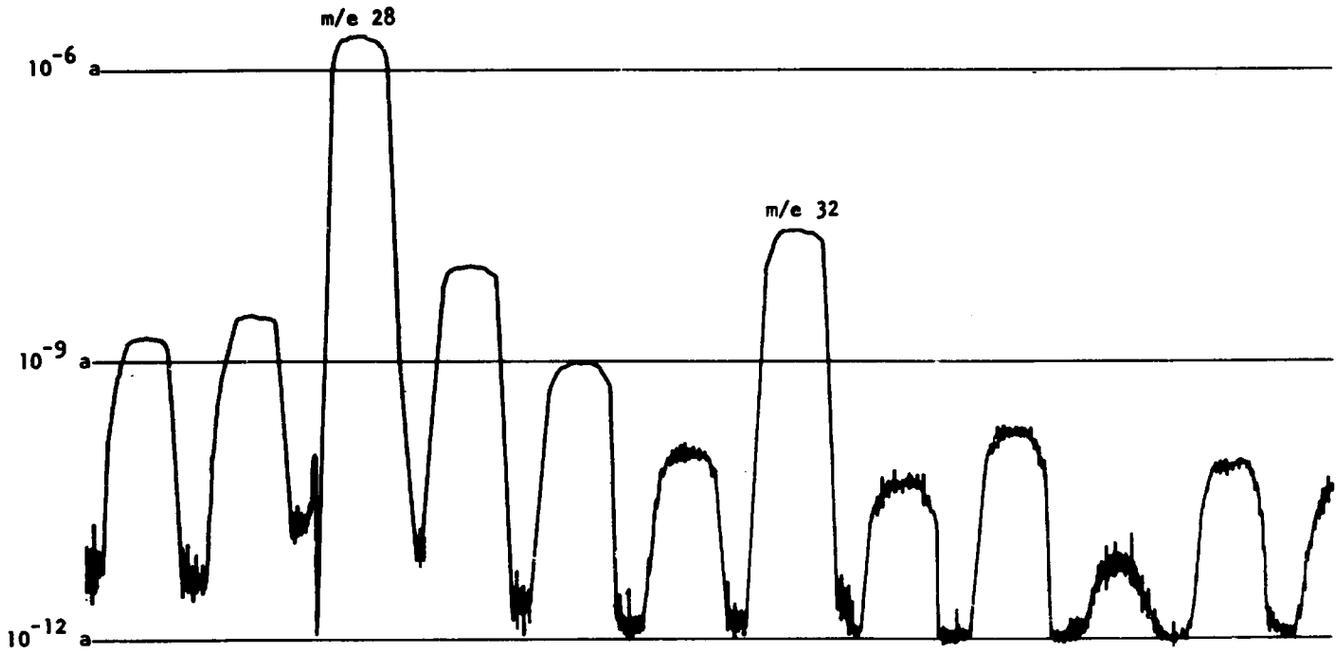

FIGURE 29. Dynamic Range

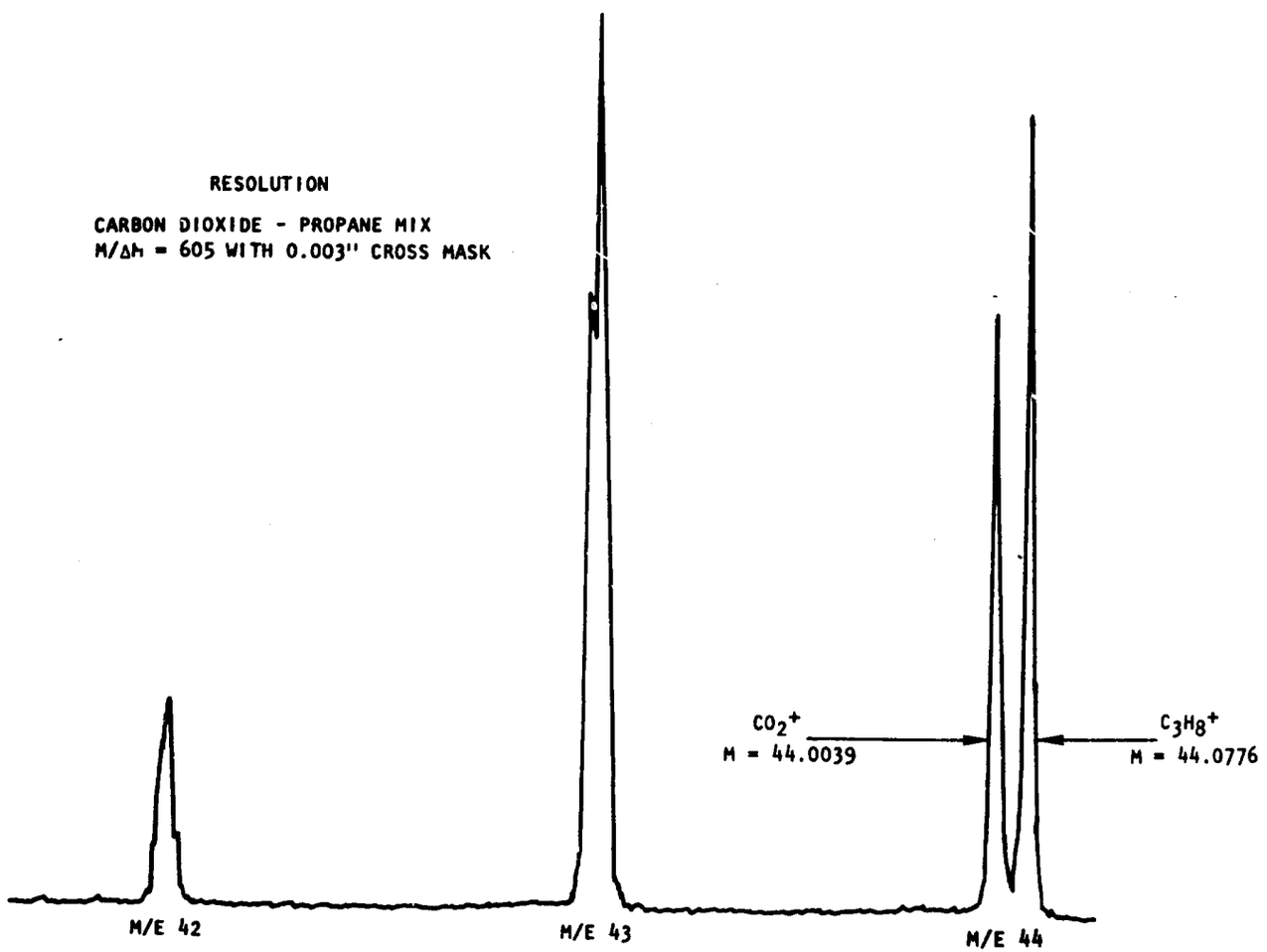

FIGURE 30. Hyperbolic Quadrupole Mass Spectrometer